THE ASTROPHYSICAL JOURNAL SUPPLEMENT SERIES, 93:397–424, 1994 August

A MORPHOLOGICAL AND COLOR STUDY OF FORNAX LOW SURFACE BRIGHTNESS GALAXIES IN THE WASHINGTON SYSTEM

SERGIO A. CELLONE[1] AND JUAN CARLOS FORTE[1]
Facultad de Ciencias Astronómicas y Geofísicas, Universidad Nacional de La Plata, Paseo del Bosque, 1900 La Plata, Argentina
AND
DOUG GEISLER
National Optical Astronomy Observatories,[2] Cerro Tololo Inter-American Observatory, Casilla 603, La Serena, Chile
Received 1993 May 27; accepted 1994 January 3

ABSTRACT

We present Washington CCD surface photometry of a sample of low surface brightness dwarf galaxies in the Fornax Cluster. Their surface brightness profiles are not always well fitted by "pure" exponential models; instead, the introduction of a shape parameter in the model profile produces very good fits. This shape parameter correlates with total magnitude; however, there may be selection effects involving the average surface brightness of the galaxies which lead to this correlation.

The color profiles of these galaxies show no meaningful gradient, except for the brightest dwarf, which shows evidence of recent or current star-forming activity at its center. Integrated colors show a dissimilar behavior: the $(M - T_1)$ index is almost constant for the whole sample, while $(C - T_1)$, which is known to be a good metallicity indicator, correlates with the structural parameters, evidencing the existence of a luminosity–metal abundance relation among these dwarfs. This relation is consistent with that already known for Local Group early-type dwarfs. No difference is found between the colors of nucleated and nonnucleated galaxies of the same luminosity.

Since total magnitudes correlate with central surface brightnesses and diameters, the more metal-rich dwarfs are also the largest and those of higher surface brightness. However, as the correlations between the different structural parameters are affected by selection effects, it is still not clear which of these parameters determines a galaxy's integrated colors, and hence its metallicity.

Subject headings: galaxies: photometry — galaxies: stellar content — galaxies: structure

1. INTRODUCTION

During the last few years, several papers have dramatically widened our knowledge about low surface brightness (LSB) dwarf galaxies. Since the first survey of Reaves (1983), both the Virgo and Fornax clusters were cataloged (Binggeli, Sandage, & Tammann 1985; Davies et al. 1988, hereafter DPCDK; Ferguson 1989, hereafter F89; Irwin et al. 1990), and other surveys included more distant clusters and poorer groups and selected areas in the general field (Karachentseva, Karachentsev, & Börngen 1985; Binggeli, Tarenghi, & Sandage 1990; Ferguson & Sandage 1990). These works showed that dwarfs represent the most numerous type of galaxy in the universe, and their importance for cosmology and galaxy evolution models has been remarked by many authors (see, for instance, Impey, Bothun, & Malin 1988, hereafter IBM).

The morphology of dwarf elliptical (dE) galaxies has been studied in some detail (Caldwell 1983; Ichikawa, Wakamatsu, & Okamura 1986; Caldwell & Bothun 1987, hereafter CB87; Bothun, Impey, & Malin 1991, hereafter BIM), as well as their optical and infrared colors (Bothun & Caldwell 1984; Thuan 1985; Bothun, Caldwell, & Schombert 1989), showing that these galaxies are systems with low surface light densities, and that their integrated colors suggest intermediately old stellar populations, with a lower than solar metallicity (but not as low as the poorer Galactic globular clusters). Spectra of a large sample of objects would be very useful to study their metallicities in detail; however, such spectra are very hard to obtain, involving long exposure times with large telescopes, and they are generally limited to bright nucleated dE's (Bothun & Mould 1988).

Multicolor CCD surface photometry of LSB galaxies is surprisingly scarce (see, for example, Vigroux et al. 1988), despite its usefulness for studying in detail the structural properties of these objects and, at the same time, providing a better knowledge of their stellar populations. It is well known that integrated optical colors do not allow one to disentangle metallicity and age effects without some assumptions. However, spectroscopic studies are not available for many LSB galaxies, and integrated photometry remains a valuable tool for a first analysis of the metallicity distribution of these objects. Among several photometric systems, the Washington system (Canterna 1976) provides a number of useful color indices that have been used for the determination of abundances in old stellar systems, including extragalactic globular clusters (Harris & Canterna 1977). In particular the $(C - T_1)$ index provides a very sensitive metallicity indicator for Galactic globular clusters (Geisler & Forte 1990).

In this work we present CCD photometry in the Washington system of a sample of 15 dE galaxies in the Fornax Cluster. The

[1] Visiting Astronomer, Cerro Tololo Inter-American Observatory, National Optical Astronomy Observatories.

[2] Operated by the Association of Universities for Research in Astronomy, Inc. (AURA, Inc.), under cooperative agreement with the National Science Foundation.

observations are summarized in § 2, and in the subsequent sections we discuss in detail the relations between their structural properties and their integrated magnitudes and colors. Possible selection effects affecting these relations are also explored. Finally, their colors are compared with those of globular clusters around bright galaxies in Fornax (Geisler & Forte 1990; Ostrov, Geisler, & Forte 1993), in order to explore possible origins common to the two kinds of objects.

2. OBSERVATIONS AND DATA REDUCTION

A sample of 15 dE galaxies was observed during two runs, in 1989 October and 1990 November, using the 0.9 m and 1.5 m telescopes at CTIO. For each galaxy, at least three CCD frames were obtained in each of the bands C, M, and T_1 of the Washington system. Individual exposure times ranged from 300 s for the brighter objects in T_1 to 900 s for the fainter ones in C. A detailed log of the observations is given in Table 1. Column (1) gives the catalog number of the galaxy (see next paragraph); column (2) gives the filter, and columns (3), (4), and (5) give the date of observation, the telescope, and the chip employed, respectively. Column (6) gives the number of frames, and column (7) is the effective exposure time. Column (8) indicates any trouble affecting the quality of the images.

The galaxies were selected from the Fornax Cluster Catalogue (F89) with the following criteria:

TABLE 1

OBSERVATIONS

Galaxy (FCC)	Filter	Date	Telescope (m)	CCD	Number	Exposure Time	Notes
76	T_1	1990 Nov	1.5	Tek	1	900	
76	C	1990 Nov	1.5	Tek	1	900	
76	M	1990 Nov	1.5	Tek	2	1200	
82	T_1	1989 Oct	0.9	TI 3	3	1800	1
82	C	1989 Oct	0.9	TI 3	3	2700	1
82	M	1990 Nov	0.9	TI 2	3	1800	
118	T_1	1989 Oct	1.5	TI 2	4	2200	
118	C	1989 Oct	1.5	TI 2	3	2550	
118	M	1990 Nov	0.9	TI 2	3	1200	
135	T_1	1989 Oct	0.9	TI 3	3	1800	
135	C	1989 Oct	0.9	TI 3	3	2700	
135	M	1990 Nov	0.9	TI 2	3	1800	
156	T_1	1990 Nov	1.5	Tek	2	1200	
156	C	1990 Nov	1.5	Tek	2	1800	
156	M	1990 Nov	1.5	Tek	2	1200	
188	T_1	1989 Oct	1.5	TI 2	3	1200	
188	C	1989 Oct	1.5	TI 2	3	1700	
195	T_1	1989 Oct	1.5	TI 2	3	1700	
195	C	1989 Oct	1.5	TI 2	3	1700	
195	M	1990 Nov	0.9	TI 2	3	1200	2
201	T_1	1990 Nov	1.5	Tek	3	1800	
201	C	1990 Nov	1.5	Tek	2	1800	
201	M	1990 Nov	1.5	Tek	1	600	
203	T_1	1989 Oct	1.5	TI 2	2	760	
203	C	1989 Oct	1.5	TI 2	3	1100	
203	M	1990 Nov	1.5	Tek	2	1200	
222	T_1	1990 Nov	1.5	Tek	2	1200	
222	C	1990 Nov	1.5	Tek	2	1800	
222	M	1990 Nov	0.9	TI 2	3	1800	
250	T_1	1990 Nov	1.5	Tek	2	1200	
250	C	1990 Nov	1.5	Tek	2	1800	
250	M	1990 Nov	1.5	Tek	2	1200	
274	T_1	1990 Nov	1.5	Tek	3	1800	
274	C	1990 Nov	1.5	Tek	3	1800	
274	M	1990 Nov	1.5	Tek	2	1200	
296	T_1	1989 Oct	0.9	TI 3	3	1800	3, 4
296	C	1989 Oct	0.9	TI 3	3	2700	3, 4
296	M	1990 Nov	0.9	TI 2	3	1800	3
303	T_1	1990 Nov	0.9	TI 2	3	900	
303	C	1990 Nov	1.5	Tek	2	1200	
303	M	1990 Nov	0.9	TI 2	3	900	
314	T_1	1989 Oct	1.5	TI 2	2	1200	
314	C	1989 Oct	1.5	TI 2	4	2300	
314	M	1990 Nov	0.9	TI 2	3	1800	

NOTES.—(1) Profile contaminated by large residuals in the flat field. (2) Frame taken with a bad focus. (3) Profile contaminated by a bright star. (4) Frame taken in nonphotometric conditions.

a) $B_{tot} < 18$, avoiding galaxies too faint for moderate-aperture telescopes.

b) Projected distance to the cluster center spans a broad range.

c) Galaxies that could be affected by nearby bright stars are excluded (by inspection with a glass magnifier of the ESO No. 358 SRC film copy).

Debiasing and flat-fielding were performed in the usual way, but as dome flats were not suited to remove low spatial frequency variations across the images, a correction using smoothed twilight sky flats was applied. This procedure resulted in very flat images (typically to 0.2% of the sky level), although low but noticeable variations are still present in a few frames (up to 0.5% or more). Since a high fraction of the luminosity of LSB galaxies arises from regions where the surface brightness is a small percentage of the sky level, we estimate that these variations account for the largest errors in our surface photometry.

Figure 1 shows halftone reproductions of square zones 90″ on a side within our corrected and co-added T_1 frames (see next section) centered on each of the galaxies.

3. SURFACE BRIGHTNESS PROFILES

3.1. *Ellipse Fitting*

Image handling was performed mainly with the IHAP package running on an HP 1000 computer at the FCAGLP and with PCVISTA and some routines of our own.

The first step for the derivation of accurate surface brightness profiles was the determination and subtraction of the sky level for each frame, which was modeled by a plane, with little or no slope. This was quite straightforward, since the target galaxies occupy only a small part of the CCD's area.

Next, all the images for a given galaxy and filter were shifted to a common reference frame, and bad pixels, both cosmetics and cosmic rays, were automatically flagged. (Bad pixels were defined as those deviating from the median by more than a value that was adjusted depending on the sky noise and the local signal.) These were afterward interactively removed by linear interpolation or local median filtering. This procedure was preferred to a median filtering of the whole image in order to avoid a further loss of resolution. Besides, our method produces frames with higher signal-to-noise ratio than the alternative procedure of taking the median of each pixel of the initial set of frames. The registered and corrected frames were added, giving as a result one frame for each galaxy in each filter, with effective exposure times ranging from 900 to 2500 s.

The low signal-to-noise ratio is the main trouble one meets with when trying to fit ellipses to the isophotes of a dE, mainly because it is difficult to determine the isophotes themselves. We tried several methods usually employed for high surface brightness (i.e., "normal") galaxies, but the best results were obtained with an iterative method adapted from Bender & Möllenhoff (1987), which permits the fitting of ellipses with varying center, semimajor axis, flattening, and position angle for each desired intensity level. The images were previously median-filtered with a 3×3 pixel window, in order to achieve a faster convergence of the iterations, but these filtered images were not used in the subsequent analysis. The results are shown in Figure 2, where the flattening b/a and position angle φ are plotted against the effective radius $r = a\sqrt{(b/a)}$. All figures correspond to parameters derived on T_1 images, and the error bars represent the standard deviation of the last five iterations.

Only two galaxies (FCC 76 and FCC 203, the first and the third ranked by total brightness) have significantly rounder isophotes for $r < 10''$, implying the existence of a bulge-type component. Other dwarfs show variations of b/a for the inner isophotes ($r < 5''$), but they may be due to the errors that arise when one tries to define an isophote with too few points, or, in the case of FCC 201, to the presence of an off-center object.

Position angles show no significant variations with r, in accordance with Ichikawa's (1989) conclusion that dE's are oblate spheroids. The only exception is perhaps (again) FCC 203, whose semimajor axis appears to tilt continuously as the isophotes get rounder. This behavior is more like that of (bright) ellipticals, which usually show isophotal twisting, as expected for triaxial objects. It should be noted that for nearly round isophotes ($b/a \simeq 0.9$), φ is poorly defined, leading to the large error bars and erratic variations seen in some of our figures.

Finally, all the galaxies have concentric isophotes, implying that none of them is noticeably deformed. (We want to stress that we did not select dwarfs seen projected near bright galaxies, in order to avoid light contamination.)

3.2. *Profile Derivation and Model Fitting*

Taking into account the small variations with r of the elliptical parameters, as discussed in the last subsection, mean values of X_0, Y_0 (the central coordinates, in pixels), b/a, and φ were adopted for each galaxy, using the isophotal level as a weight. This procedure gives results that are not affected by the outermost (and then noisier) isophotes; the innermost ones, defined by too few pixels, were simply discarded. In every case, we checked the fits interactively, also discarding any isophote affected by a bright object. Normally, the mean values were similar within the errors for C, M, and T_1, so T_1 values were adopted for the three bands.

With these mean parameters, the growth curve (i.e., the integrated flux as a function of r) and the instrumental surface brightness profile were derived for each galaxy, independently in C, M, and T_1. As Binggeli, Sandage, & Tarenghi (1984) show in their Figure 2, small errors in the adopted sky level may give as a result growth curves that depart from the expected asymptotic behavior. For some of our frames, the initially adopted sky level was too high, so its value was slightly changed until a flat growth curve was obtained. From this new growth curve, a corrected surface brightness profile was derived.

The instrumental profiles were transformed into the Washington system through the observation of between 5 and 11 standard stars per night, taken from the lists of Geisler (1990). Mean extinction coefficients for CTIO were adopted; typical errors in the calibration equations amount to 0.01 mag in T_1 and 0.03 mag in $(C - T_1)$. The resulting standard profiles are displayed in Figure 3, where the surface brightness in T_1 mag arcsec^{-2} is plotted against the equivalent radius r in a linear scale. With this scale, an exponential profile gives a straight line, and what is readily seen is that all the galaxies in this

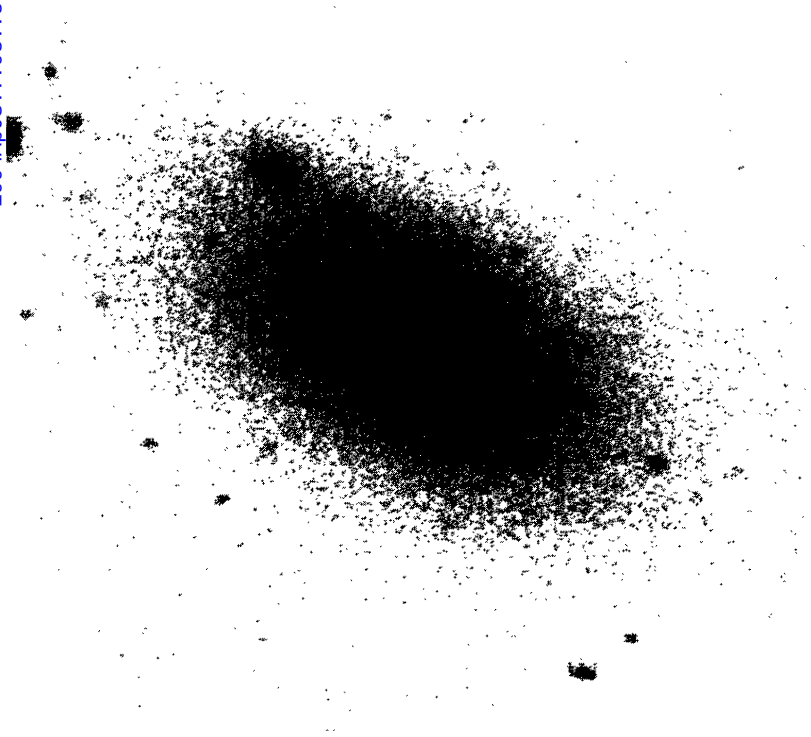

FIG. 1*a*

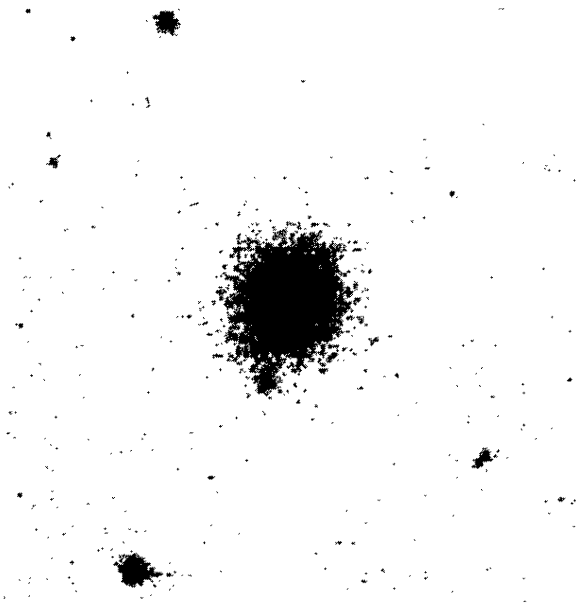

FIG. 1*b*

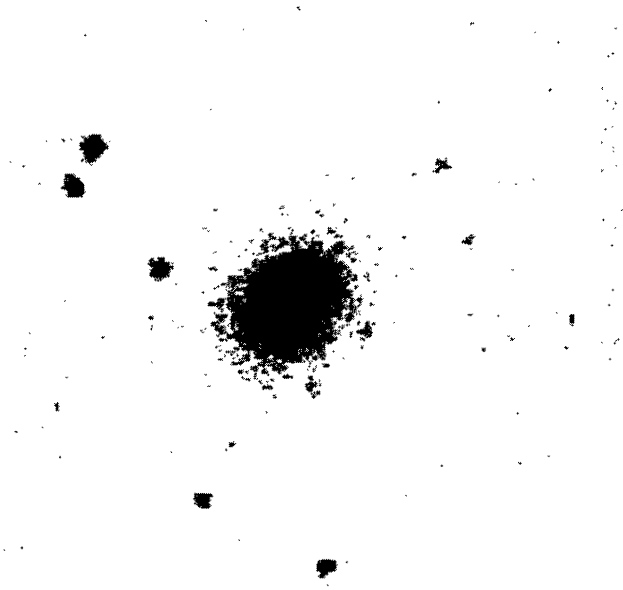

FIG. 1*c*

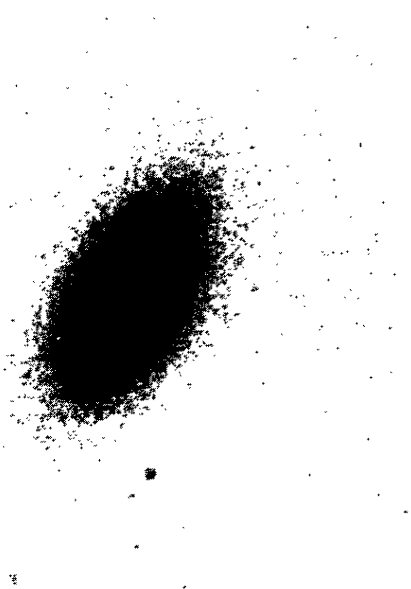

FIG. 1*d*

FIG. 1.—CCD images of the observed galaxies (T_1 band). Each frame is 90″ on a side, except for (*a*), which is 120″ on a side. North is up, and east is to the left in all pictures. (*a*) FCC 76, (*b*) FCC 82, (*c*) FCC 118, (*d*) FCC 135, (*e*) FCC 156, (*f*) FCC 188, (*g*) FCC 195, (*h*) FCC 201, (*i*) FCC 203, (*j*) FCC 222, (*k*) FCC 250, (*l*) FCC 274, (*m*) FCC 296, (*n*) FCC 303, (*o*) FCC 314.

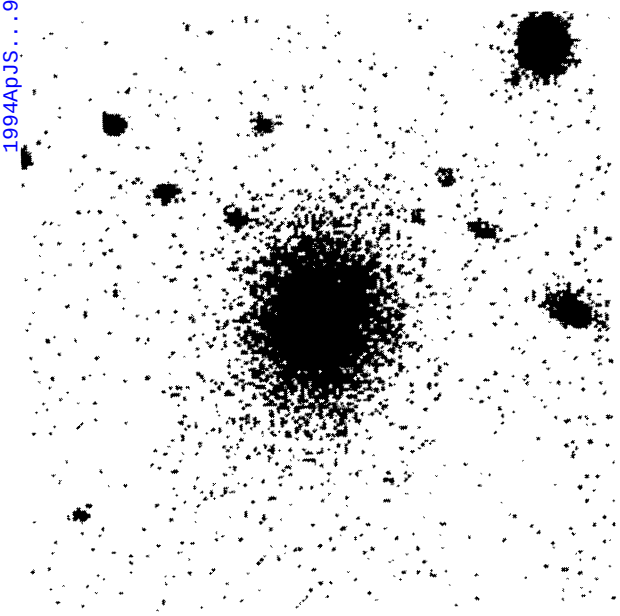

FIG. 1*e*

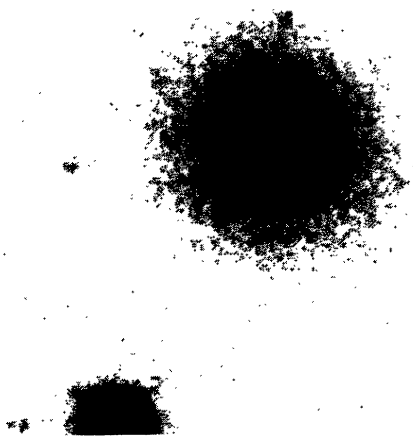

FIG. 1*f*

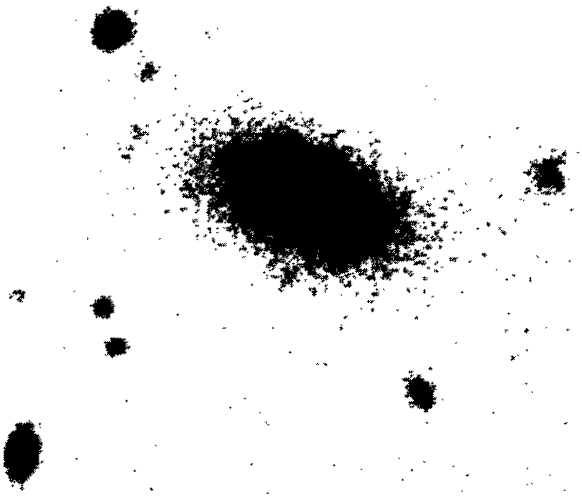

FIG. 1*g*

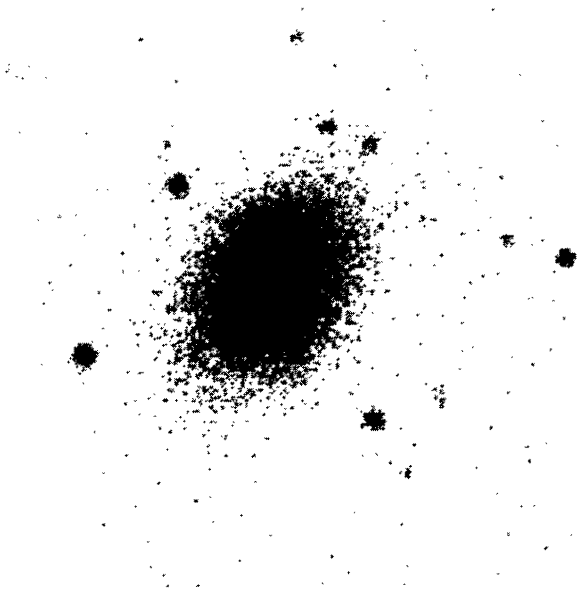

FIG. 1*h*

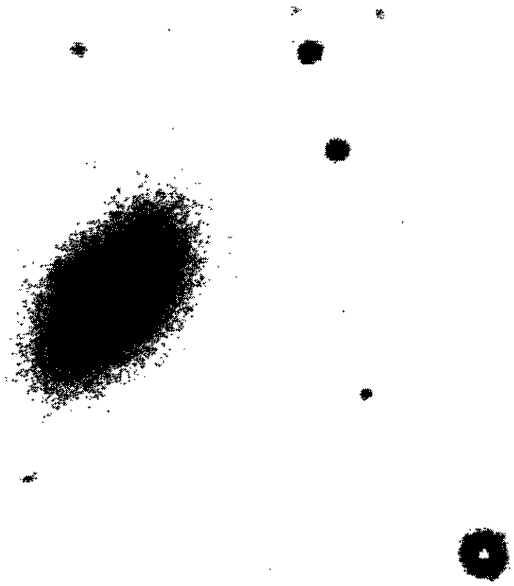

FIG. 1*i*

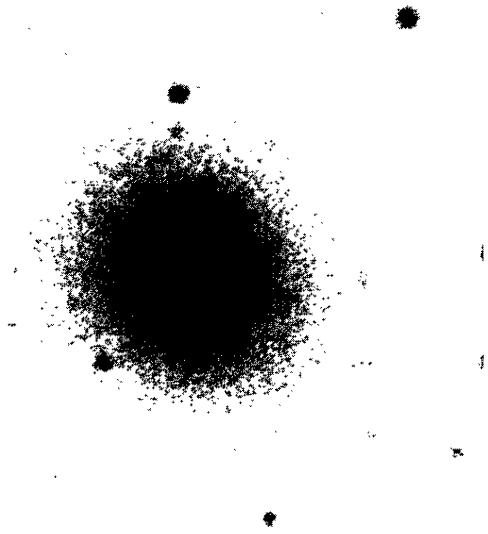

FIG. 1*j*

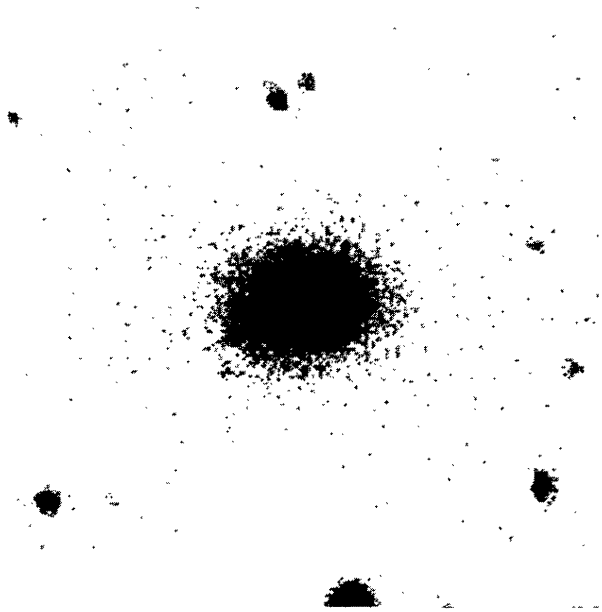

FIG. 1*k*

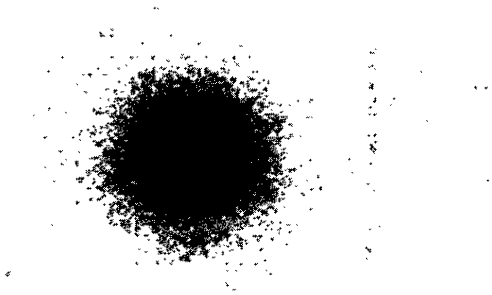

FIG. 1*l*

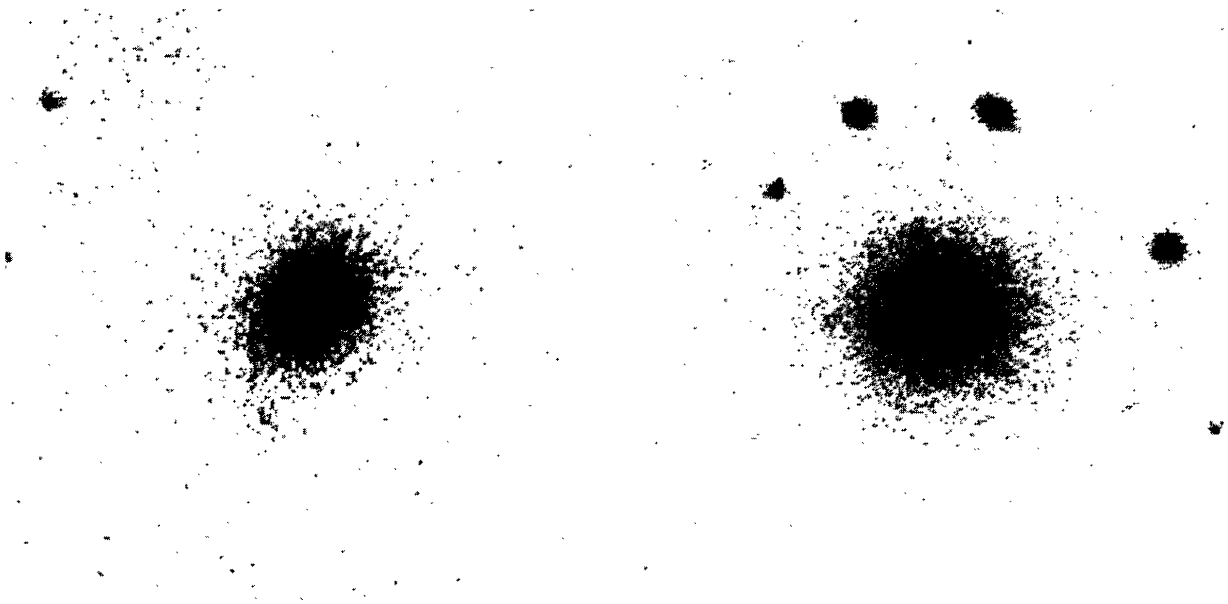

FIG. 1*m*

FIG. 1*n*

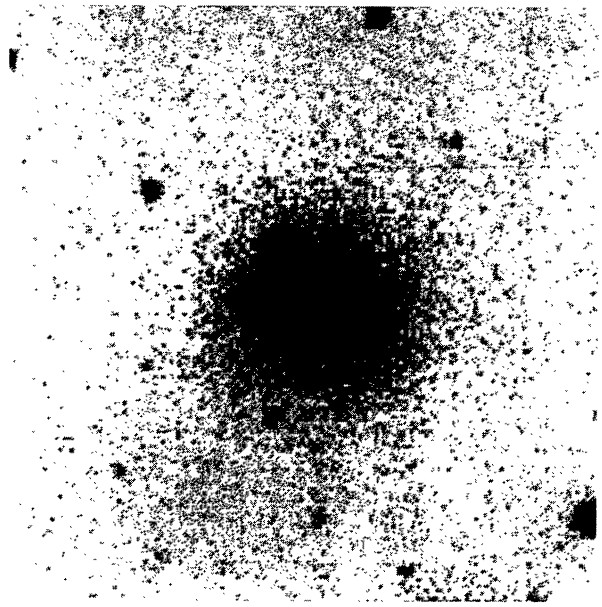

FIG. 1*o*

sample roughly behave like that, in agreement with previous works (Karachentseva, Schmidt, & Richter 1984; Binggeli et al. 1984; Ichikawa et al. 1986; CB87; IBM). However, a careful inspection of Figure 3 shows that only a small fraction of all profiles can be regarded to as "pure" exponentials, since most of them depart from a straight line in either one or the other direction. This fact was also noticed by other authors (Karachentseva et al. 1987; CB87; IBM), who showed that brighter dE's tend to have a bulge component, and so their profiles resemble more an $r^{1/4}$ law, while the fainter dwarfs usually have large cores, i.e., their profiles show a curvature in the opposite way.

In order to study this effect quantitatively, the standard profiles were fitted with a generalized exponential model:

$$I(r) = I_0 \exp\left[-\left(\frac{r}{\alpha}\right)^N\right], \qquad (1)$$

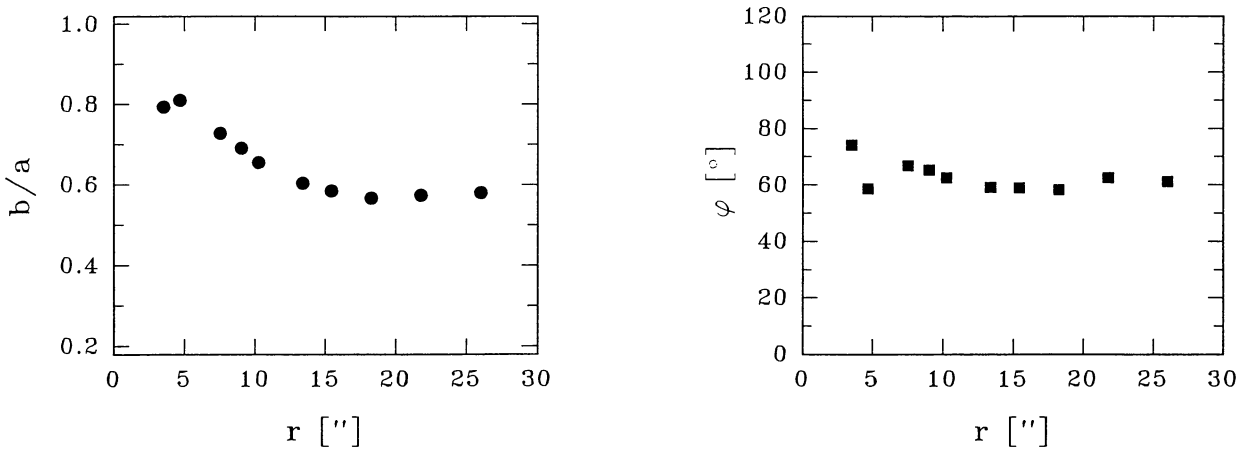

FIG. 2a

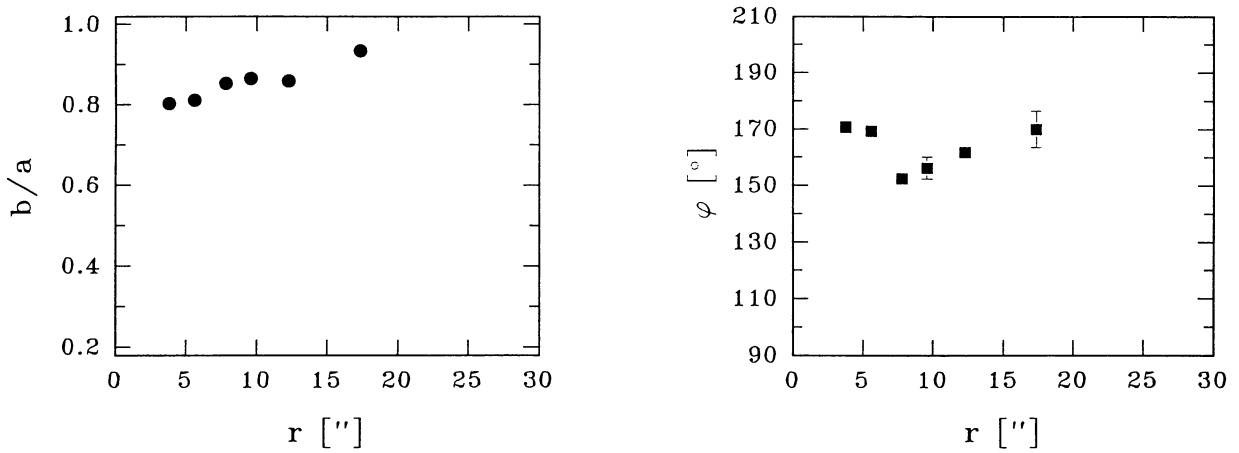

FIG. 2b

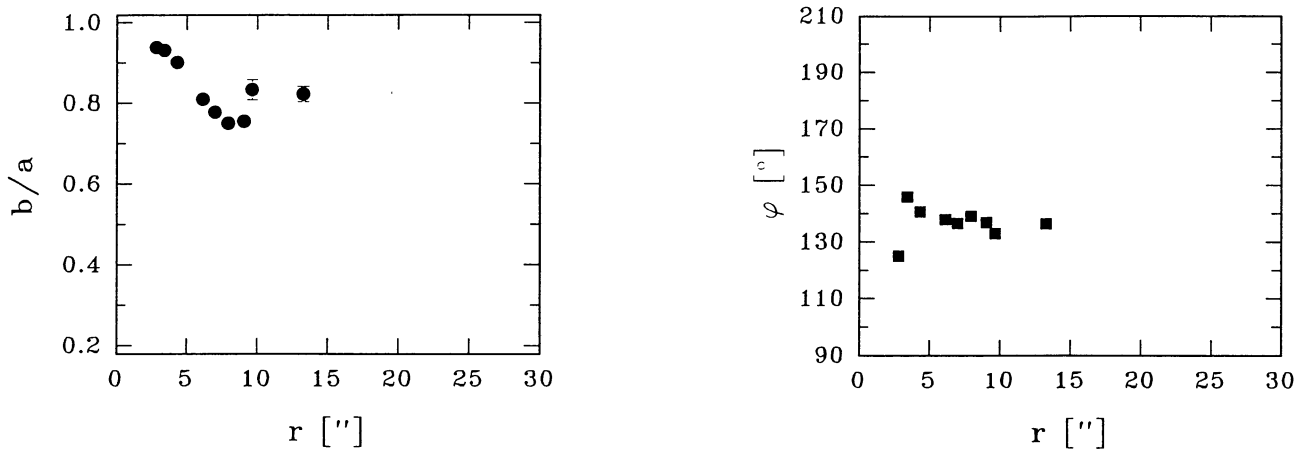

FIG. 2c

FIG. 2.—Apparent flattening (b/a) and position angle of the semimajor axis (φ) plotted against the equivalent radius (r) in arcseconds. Position angles are measured from north through east. The error bars (not shown when the error is smaller than the symbol size) represent the standard deviation of the last five iterations (see text). (*a–o*) Same as in Fig. 1.

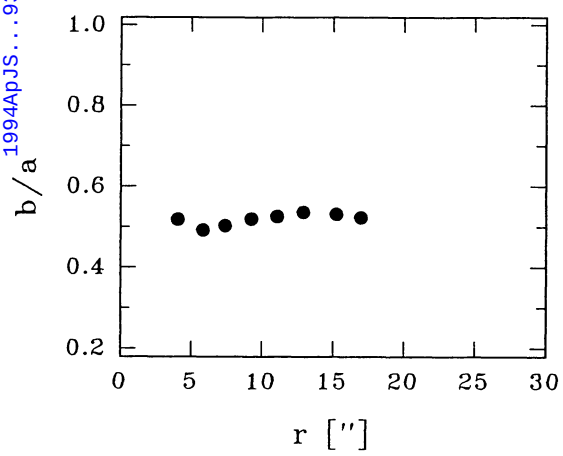

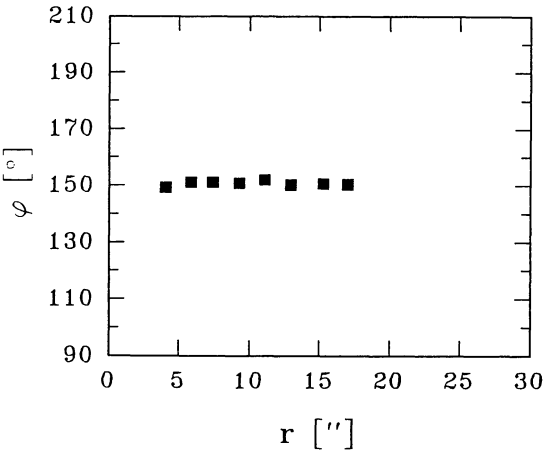

FIG. 2*d*

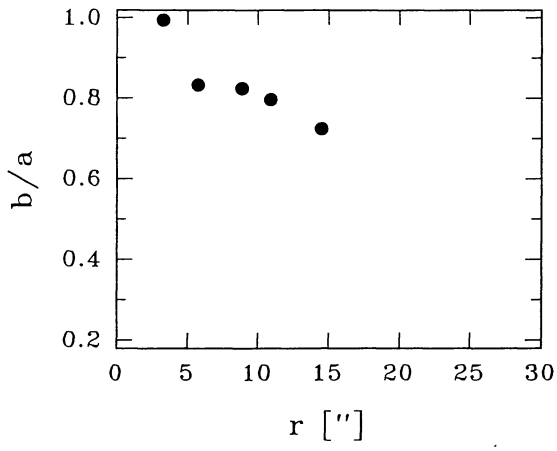

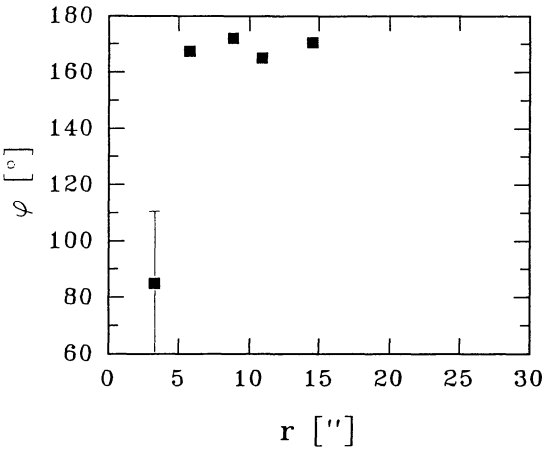

FIG. 2*e*

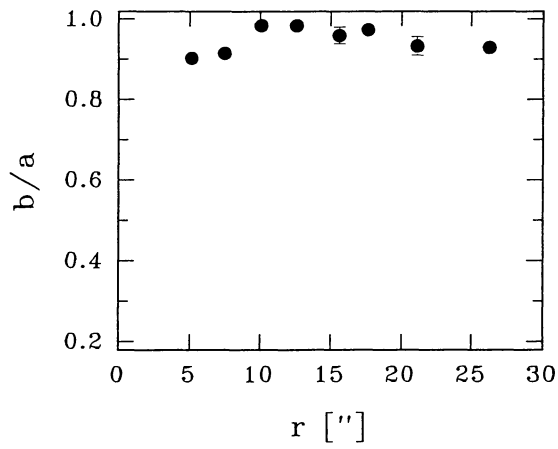

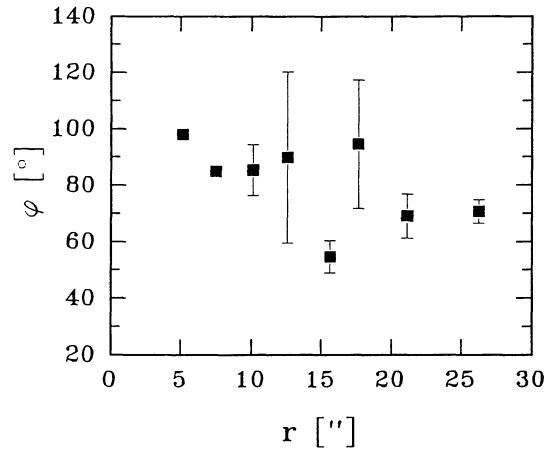

FIG. 2*f*

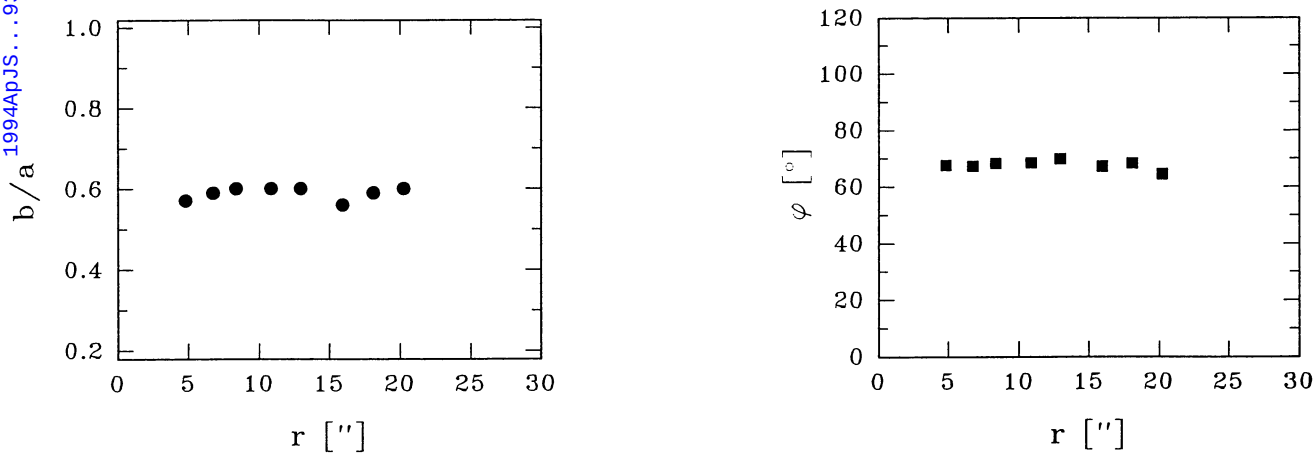

FIG. 2*g*

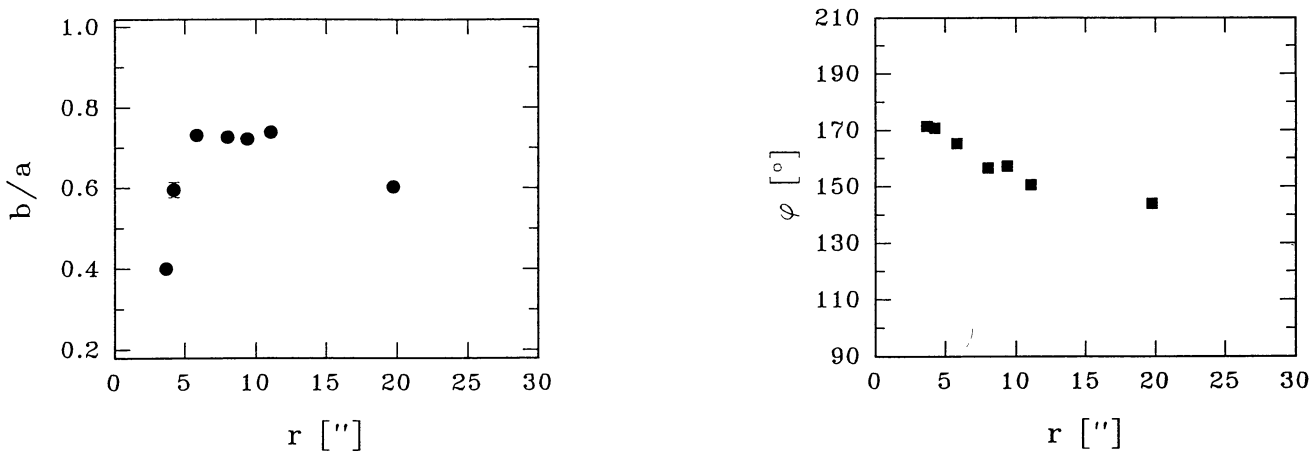

FIG. 2*h*

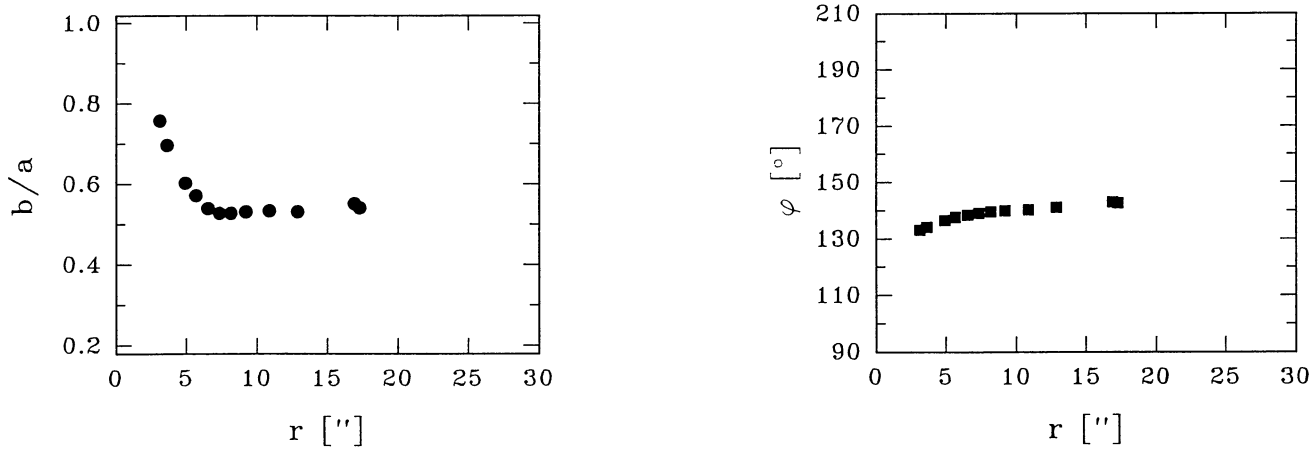

FIG. 2*i*

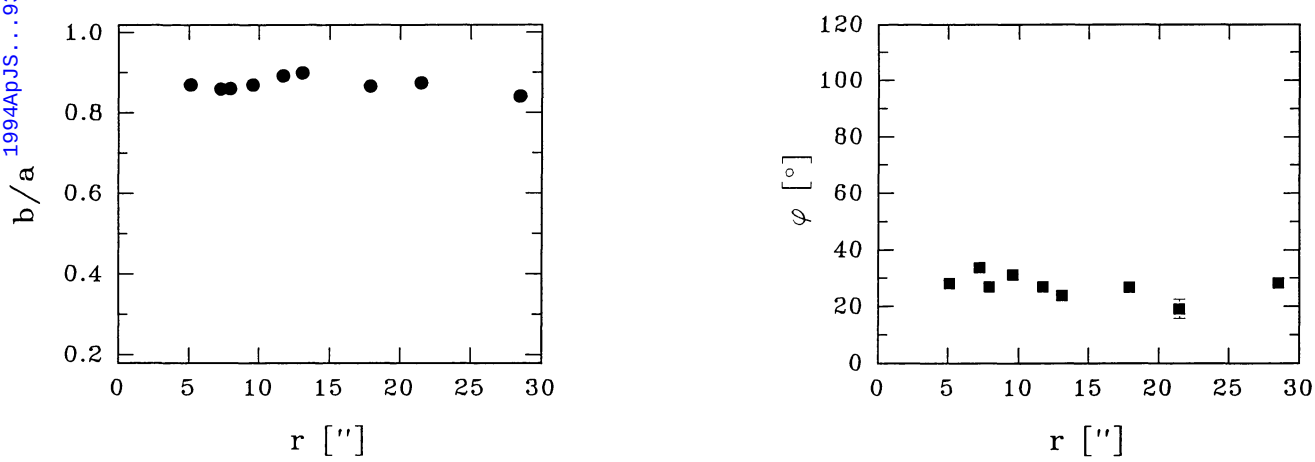

FIG. 2*j*

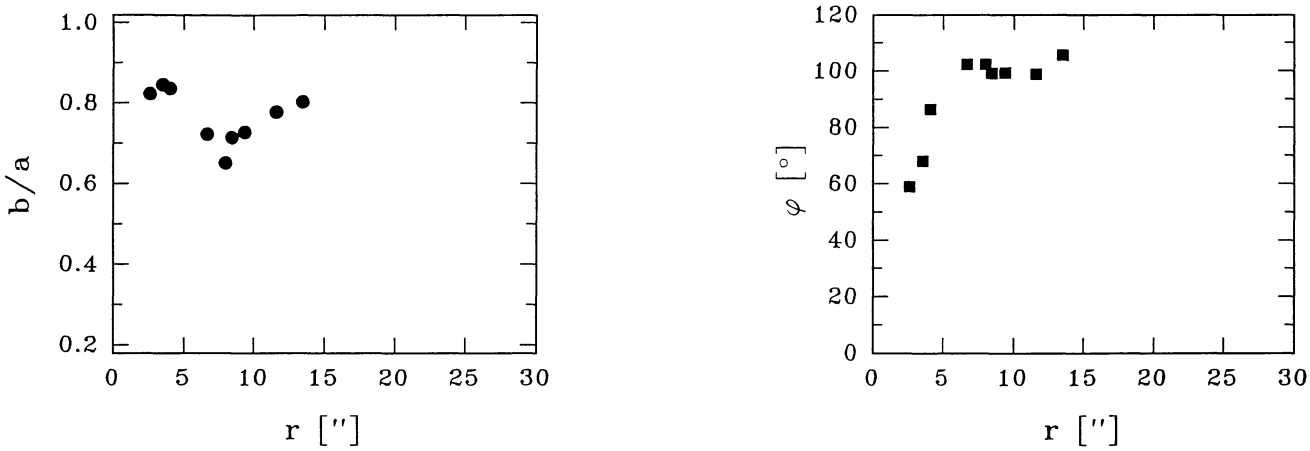

FIG. 2*k*

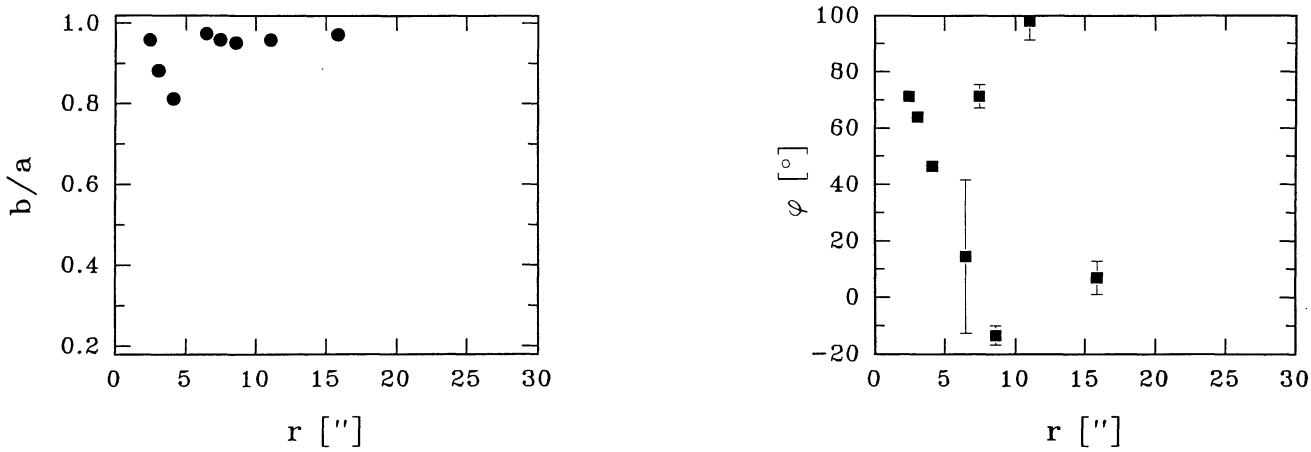

FIG. 2*l*

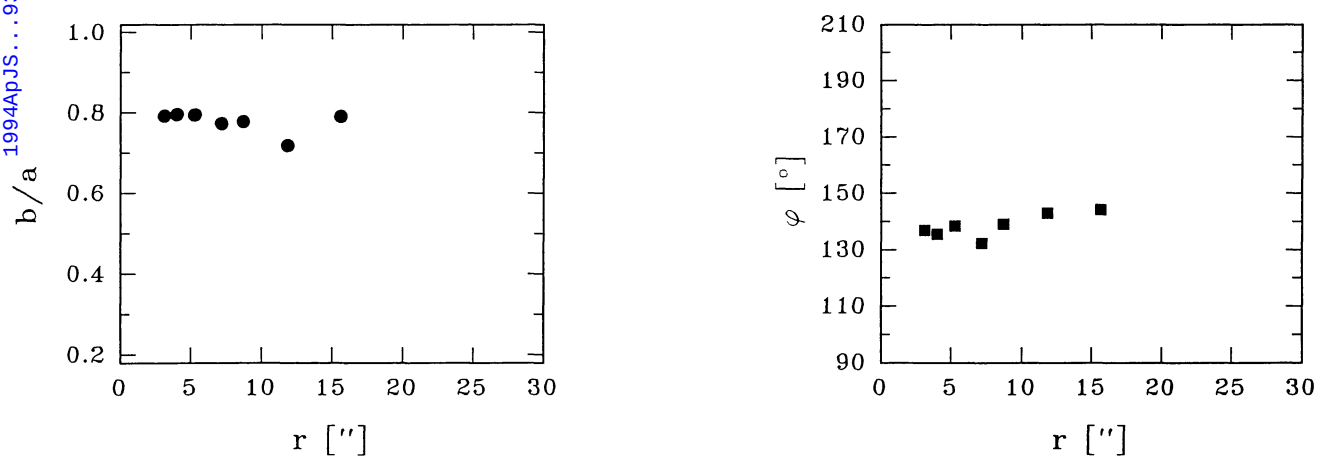

FIG. 2*m*

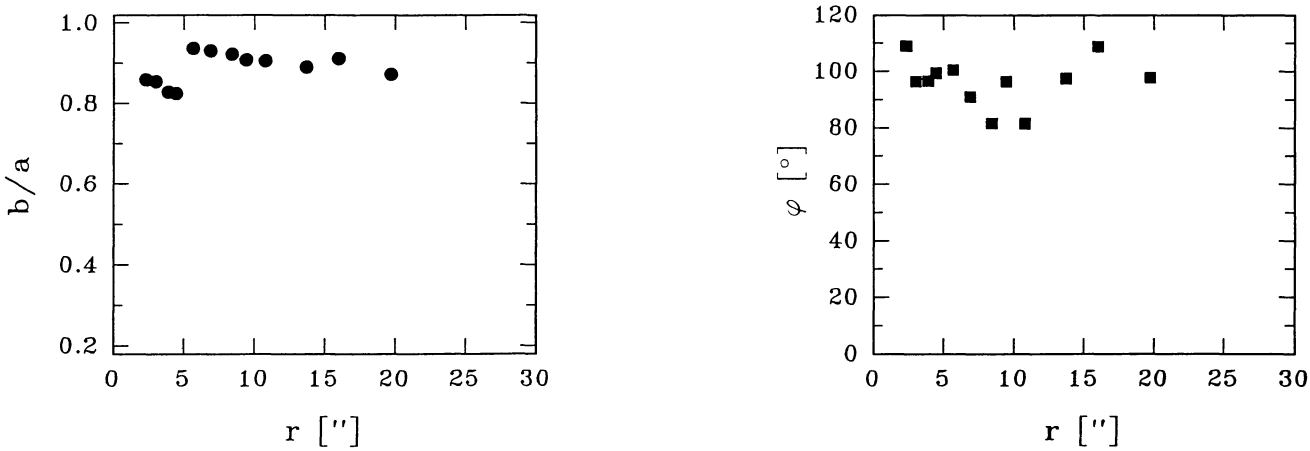

FIG. 2*n*

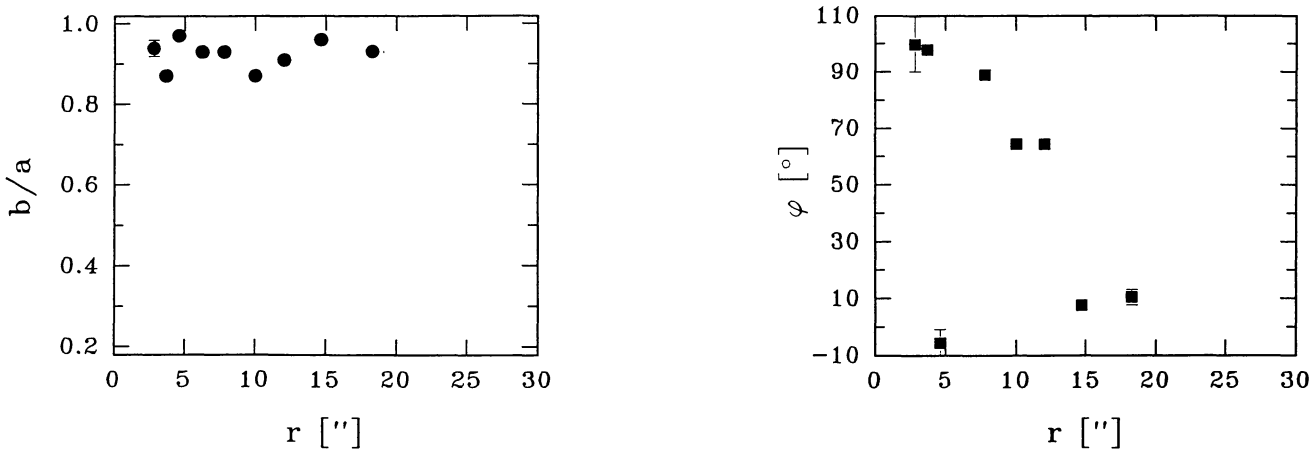

FIG. 2*o*

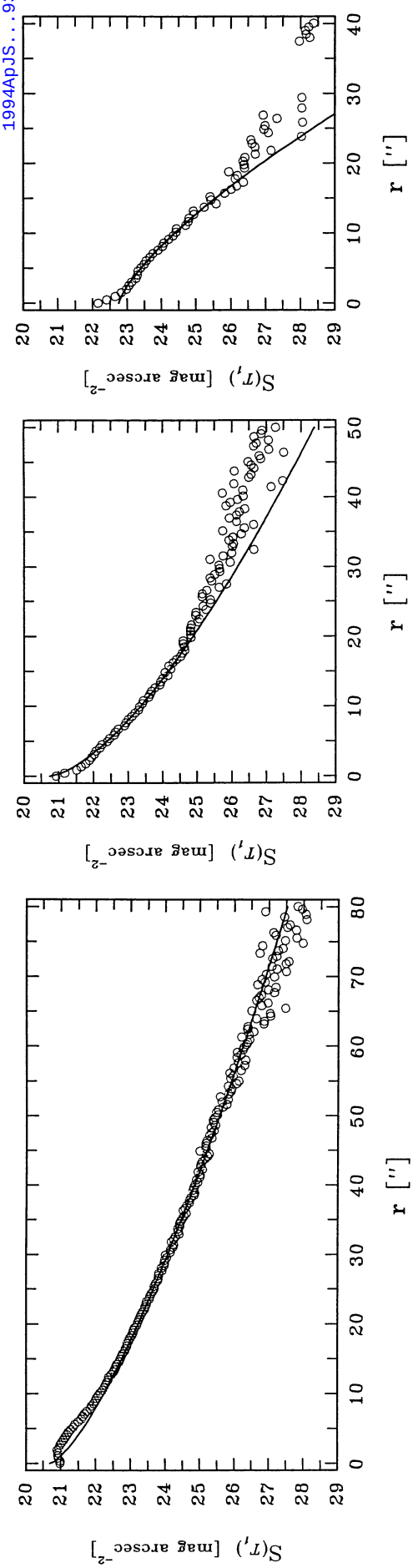

FIG. 3.—Surface brightness (*circles*) and color [$(M - T_1)$: *squares*; $(C - T_1)$: *triangles*] profiles as a function of equivalent radius (r) in arcseconds. Solid lines show the fitted models. (*a–o*) Same as in Fig. 1.

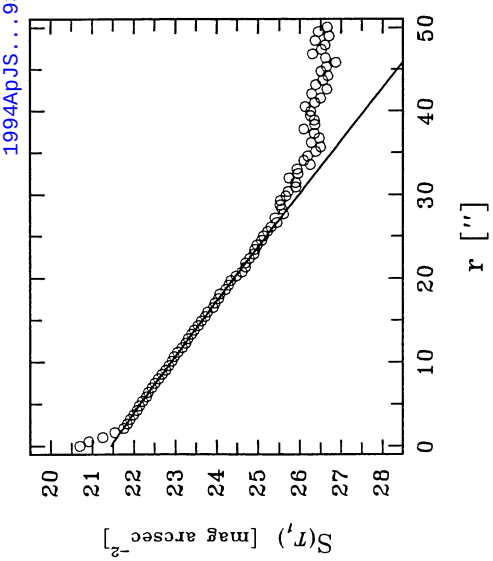

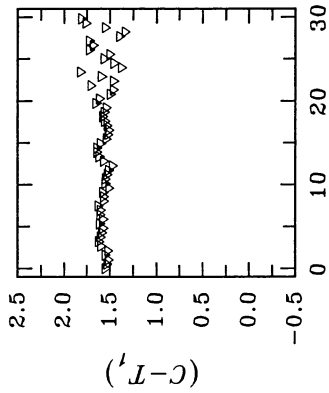

FIG. 3f

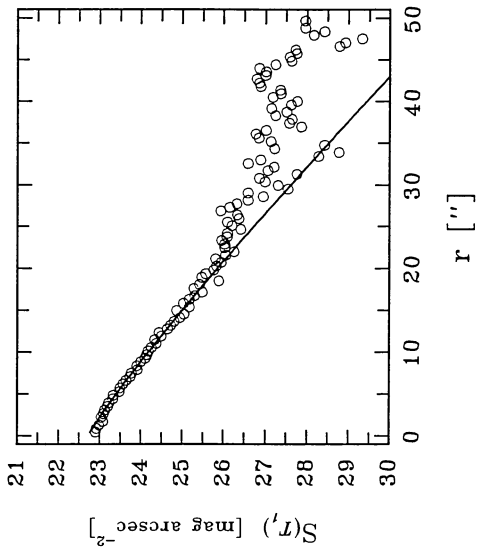

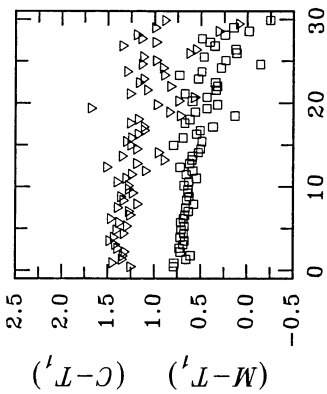

FIG. 3e

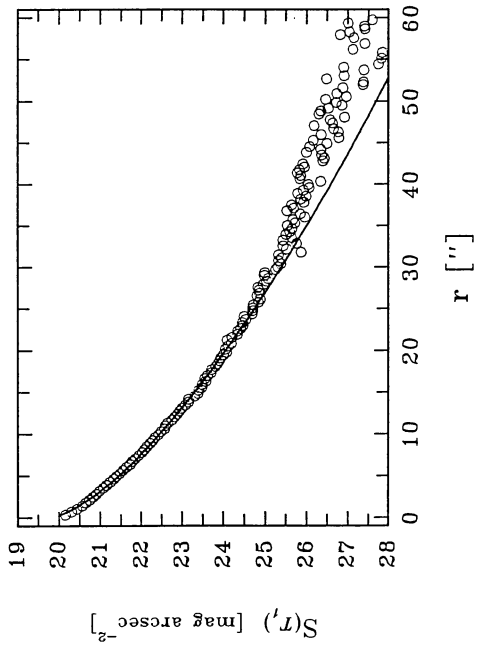

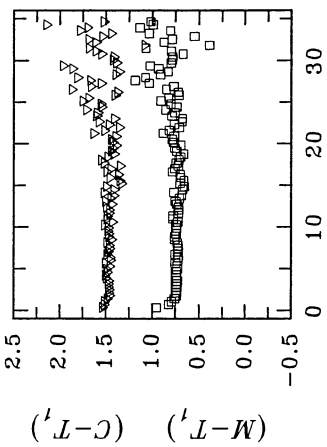

FIG. 3d

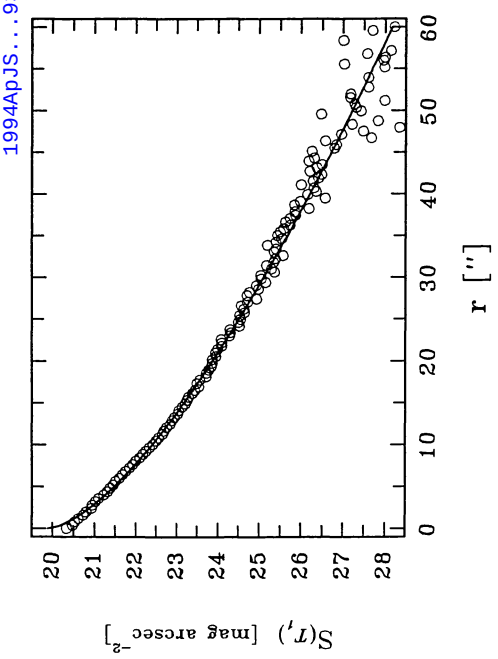

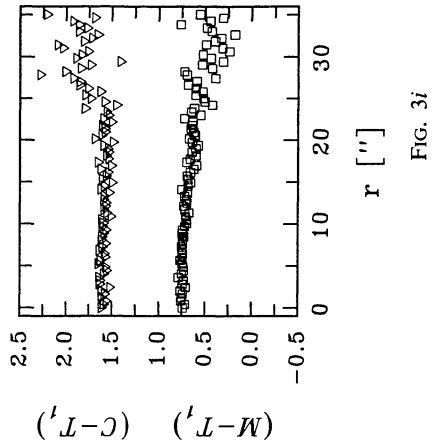

FIG. 3*i*

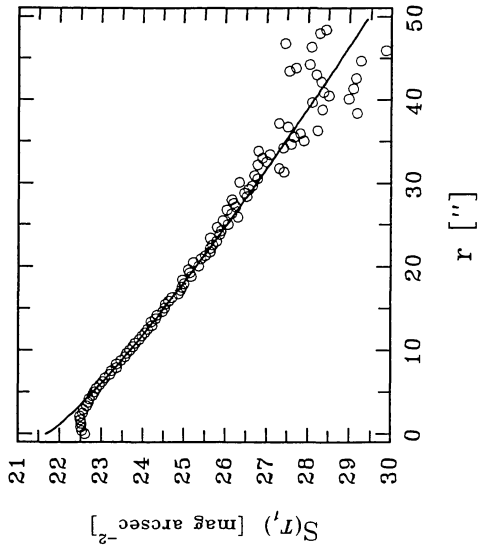

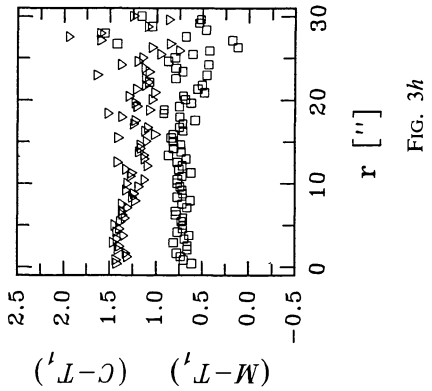

FIG. 3*h*

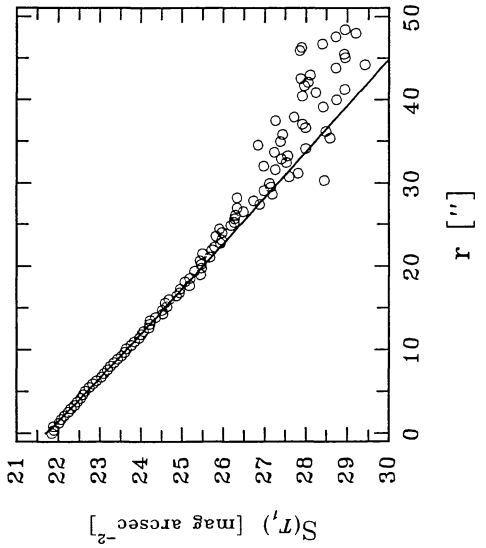

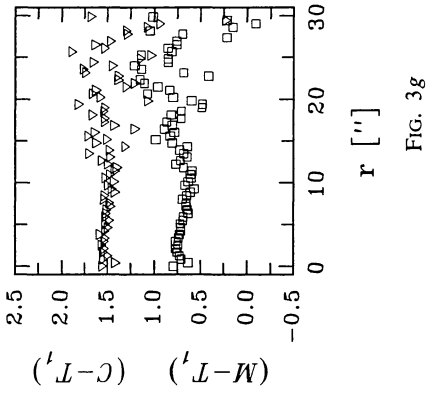

FIG. 3*g*

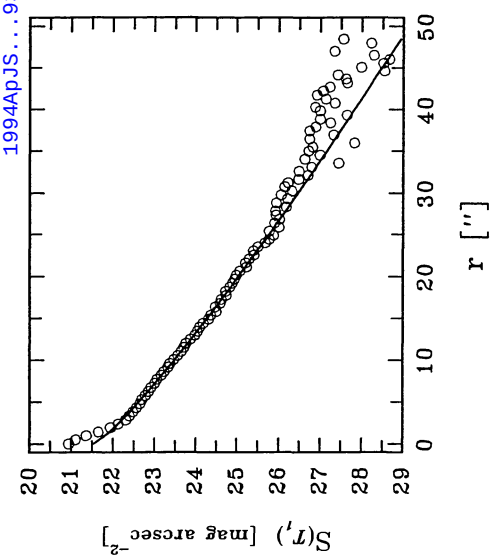

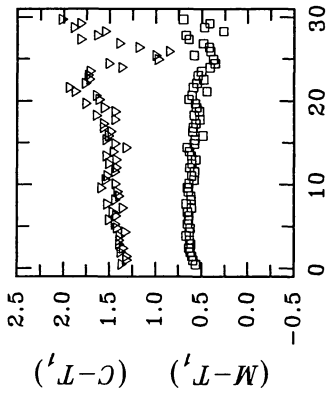

FIG. 3*l*

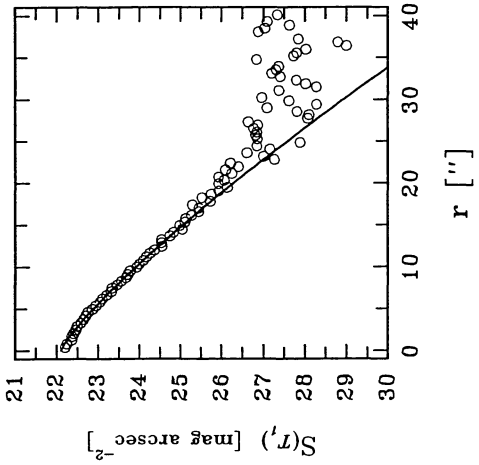

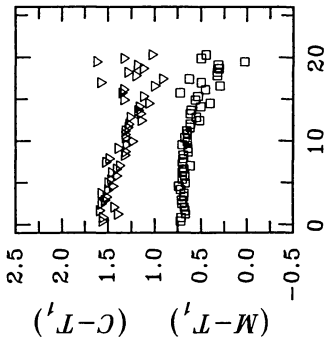

FIG. 3*k*

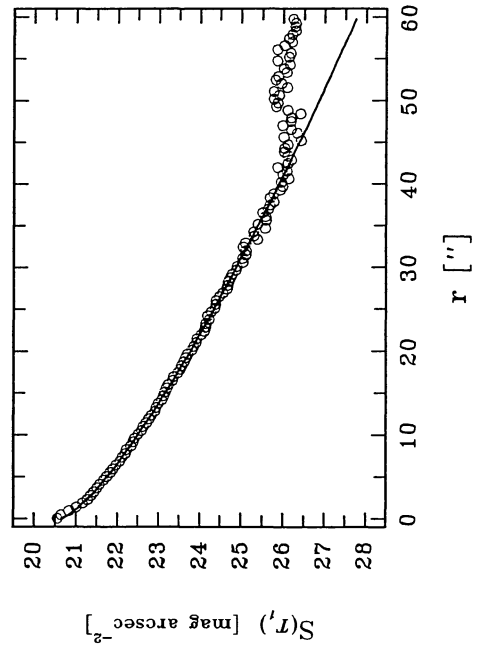

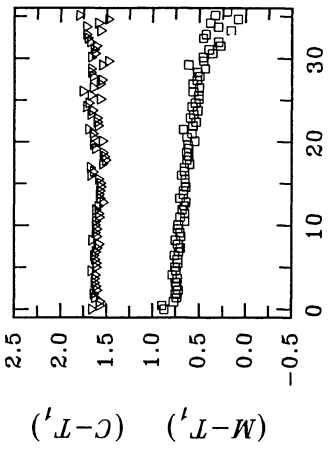

FIG. 3*j*

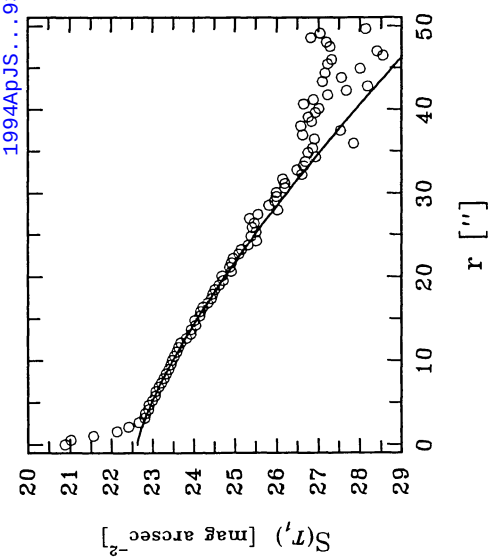

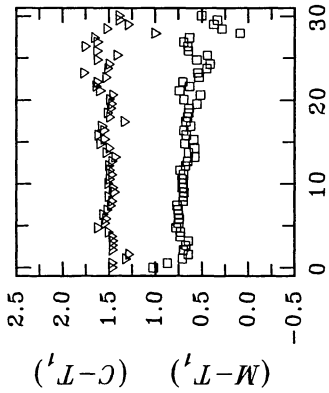

FIG. 3o

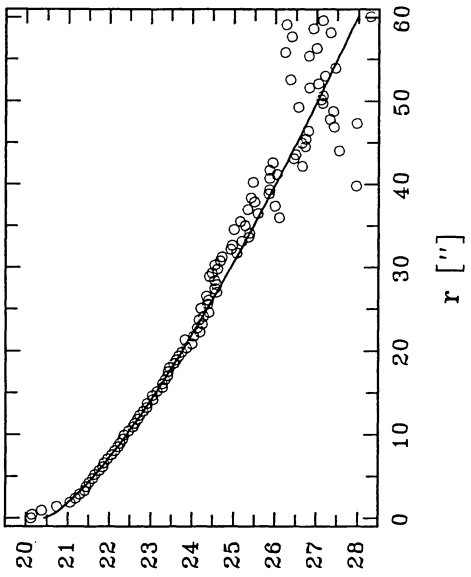

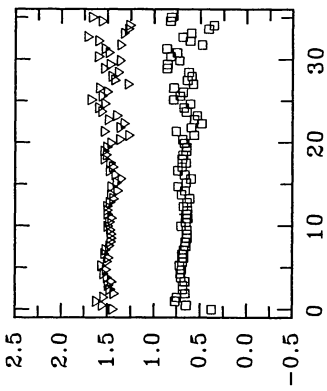

FIG. 3n

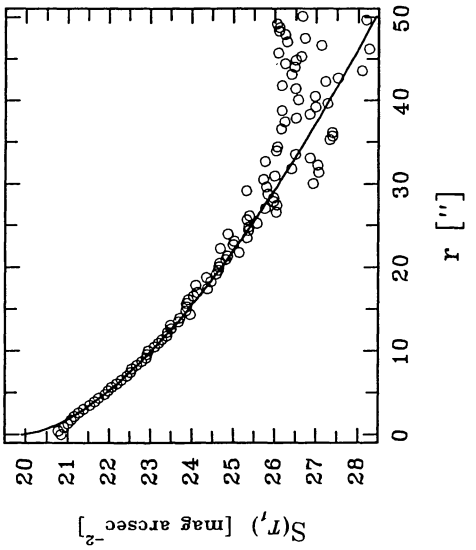

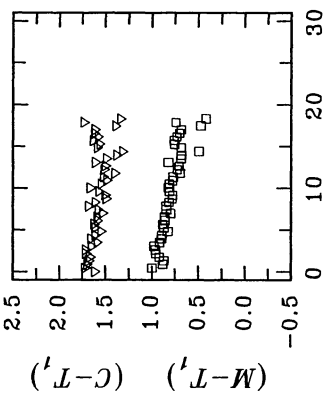

FIG. 3m

TABLE 2

STRUCTURAL PARAMETERS

Galaxy (FCC)	$S_{0(T_1)}$ (mag/arcsec^{-2})	α	N	Nucleus[a]
76	20.69 ± 0.34	6".12 ± 1".70	0.72 ± 0.06	...
82	20.74 ± 0.26	2.68 ± 0.80	0.67 ± 0.07	(Nuc)
118	22.75 ± 0.24	7.43 ± 1.21	1.35 ± 0.21	Nuc
135	19.75 ± 0.06	2.58 ± 0.16	0.67 ± 0.01	...
156	22.73 ± 0.11	7.67 ± 0.74	1.10 ± 0.10	...
188	21.46 ± 0.06	7.65 ± 0.34	1.04 ± 0.03	Nuc
195	21.70 ± 0.06	5.49 ± 0.32	0.97 ± 0.03	...
201	21.68 ± 0.15	4.80 ± 0.67	0.84 ± 0.06	...
203	19.90 ± 0.07	2.90 ± 0.22	0.67 ± 0.02	...
222	20.66 ± 0.06	4.94 ± 0.31	0.75 ± 0.02	(Nuc)
250	22.11 ± 0.05	6.56 ± 0.28	1.21 ± 0.05	...
274	21.54 ± 0.13	5.04 ± 0.61	0.85 ± 0.05	Nuc
296	19.91 ± 0.23	1.86 ± 0.51	0.63 ± 0.06	...
303	20.44 ± 0.13	4.48 ± 0.62	0.75 ± 0.04	Nuc
314	22.63 ± 0.06	12.00 ± 0.54	1.31 ± 0.07	Nuc

[a] (Nuc) means a dubious case.

where I is the surface brightness in intensity units, and I_0, α, and N are free parameters, namely, the central surface brightness, the scale length, and an exponent that governs the profile shape. In particular, $N = 1$ implies a "pure" exponential, while $N = 0.25$ is a de Vaucouleurs profile, commonly used for gE galaxies.

The surface brightness in magnitudes per square arcsecond is then given by

$$S(r) = S_0 + 1.086\left(\frac{r}{\alpha}\right)^N. \quad (2)$$

In practice, the fit is made in this domain.

Figure 3 also shows the fitted models as solid lines. We want to emphasize that only those regions of each galaxy where the profile is well defined were used to make the fits, avoiding in this way the nuclei (when present) and the outer regions where background objects or the seeing wings of foreground stars contaminate the profiles. Table 2 lists the fitted structural parameters for the 15 galaxies in our sample, corresponding to the T_1 images. The quoted uncertainties are the formal errors of the fitting procedure.

In what follows we discuss the different definitions of the derived parameters (total magnitudes, surface brightnesses, and sizes; see Table 3) and the relations we find between them.

4. STRUCTURAL PROPERTIES

4.1. *Integrated Magnitudes*

The total magnitude integrated from the analytical profile is

$$m_{\rm tot} = S_0 - 2.5\log(2\pi\alpha^2) - 2.5\log\left[\frac{\Gamma(2/N)}{N}\right], \quad (3)$$

where Γ is the gamma function and the integration is carried out to infinity. This magnitude can be easily calculated from the model parameters, which are in turn derived from the higher signal-to-noise (and therefore less affected by errors) regions of the galaxy, but it does not take into account features that may occur in a real galaxy, such as a nucleus or structural components not fitted by the model.

A magnitude integrated within a given isophote from the radial profile has none of the disadvantages mentioned for $m_{\rm tot}$, but care should be taken in selecting an appropriate isophote: a bright one will not include most of the galaxy, and one too faint may be poorly defined. Inspection of Figure 3 reveals that all the profiles are well defined down to $S \simeq 26$ mag arcsec^{-2}, so we adopted this isophote to measure our $T_{1_{26}}$ magnitudes. Comparing our T_1 total magnitudes with the B magnitudes listed by DPCDK and F89, we find $(B - T_1) = 1.08 \pm 0.20$ and 0.93 ± 0.16, respectively, and then our isophotal limit roughly matches the isophotal detection limit $S_{(B)} = 27$ mag arcsec^{-2} in F89.

TABLE 3

DERIVED PARAMETERS

Galaxy (FCC)	r_{26}	$T_{1_{\rm tot}}$ (mag)	$T_{1_{26}}$ (mag)	$S_{26(T_1)}$ (mag/arcsec^{-2})
76	56".19 ± 0".74	13.84 ± 0.03	13.95 ± 0.03	23.94 ± 0.004
82	28.54 ± 0.74	15.41 ± 0.06	15.55 ± 0.05	24.07 ± 0.003
118	16.69 ± 0.73	16.86 ± 0.09	17.03 ± 0.08	24.38 ± 0.012
135	34.98 ± 1.03	14.53 ± 0.07	14.61 ± 0.07	23.57 ± 0.001
156	20.85 ± 0.96	16.49 ± 0.09	16.71 ± 0.09	24.55 ± 0.015
188	30.13 ± 0.33	15.13 ± 0.03	15.21 ± 0.02	23.84 ± 0.001
195	22.74 ± 0.43	15.94 ± 0.04	16.07 ± 0.04	24.10 ± 0.001
201	24.80 ± 0.49	15.87 ± 0.04	16.07 ± 0.04	24.29 ± 0.001
203	38.06 ± 0.69	14.43 ± 0.04	14.53 ± 0.04	23.68 ± 0.001
222	40.95 ± 0.43	14.45 ± 0.02	14.61 ± 0.02	23.92 ± 0.001
250	18.87 ± 0.41	16.35 ± 0.05	16.48 ± 0.04	24.10 ± 0.005
274	26.68 ± 0.45	15.65 ± 0.04	15.75 ± 0.04	24.13 ± 0.001
296	29.25 ± 0.71	15.11 ± 0.05	15.22 ± 0.05	23.79 ± 0.003
303	39.88 ± 0.66	14.42 ± 0.04	14.53 ± 0.03	23.78 ± 0.002
314	28.45 ± 0.76	15.66 ± 0.05	15.74 ± 0.05	24.25 ± 0.011

NOTE.—The quoted errors were estimated by changing the parameters of the models by reasonable amounts.

$T_{1_{26}}$ can be measured directly from the real profile, or it can alternatively be integrated with the model parameters. The average difference in absolute value between both determinations of $T_{1_{26}}$ is 0.025 ± 0.016 mag; this error can be completely accounted for by the sky noise, showing that the amount of light coming from galaxy components deviating from the model is negligible. It should be noted that, in both cases, the isophotal radius r_{26} was determined from the model.

Figure 4 shows that a very tight correlation exists between our $T_{1_{26}}$ and $T_{1_{tot}}$ magnitudes; however, this simply means that we have chosen an isophote ($S = 26$ mag arcsec^{-2}) that encompasses most of the light (typically 90%) for all the galaxies. The superposed solid curves in the same figure correspond to exponential models with the same α, while the dashed lines correspond to the same S_0. It is evident that models with $S_0 <$ 24 mag arcsec^{-2} lie within a very narrow strip in this plot, explaining the mentioned correlation for our galaxies [$S_{0_{(T_1)}} \leq$ 22.75]. Instead, for galaxies with fainter S_0, the $S = 26$ isophote encompasses only a small fraction of the total luminosity, and so a fainter isophote should be selected. (Obviously no galaxy can exist with $T_{1_{26}}$ brighter than $T_{1_{tot}}$.) The curves were drawn for $N = 1$, but similar results are obtained with N varying within a range encompassing all our observed values.

So, for our galaxies $T_{1_{26}}$ or $T_{1_{tot}}$ could be used interchangeably; however, in what follows we shall use $T_{1_{tot}}$ because it can be more directly compared with total blue magnitudes used in most other works.

4.2. *Central and Average Surface Brightnesses*

The extrapolated central surface brightness (S_0), derived from the exponential fit to the profile, has been often used as a structural parameter characterizing a given galaxy. IBM pointed out its advantages compared with, for example, the mean surface brightness within the effective radius $\langle S_e \rangle$, but it should be noted that the extrapolation of the exponential fit to the center of the galaxy ignores any nucleus or bulge component.

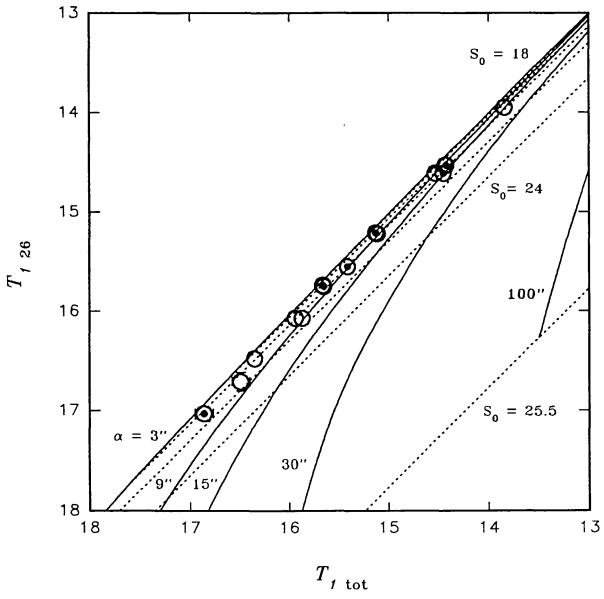

FIG. 4.—$T_{1_{26}}$ magnitudes vs. $T_{1_{tot}}$. Dotted circles represent nucleated dwarfs. The error bars correspond to the uncertainties listed in Tables 2 and 3; they are not shown when the symbol size is larger than the error. The solid lines show the locus of exponential models ($N = 1$) with the same scale length (α), while dashed lines are those with the same central surface brightness (S_0).

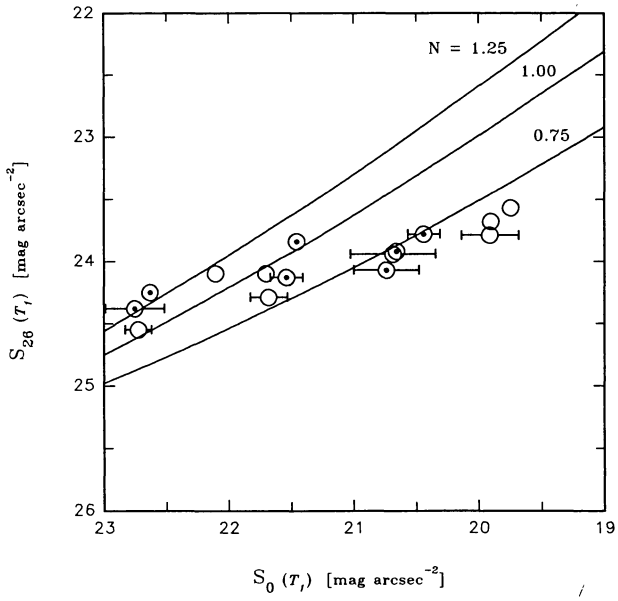

FIG. 5.—Mean surface brightness within the $S = 26$ mag arcsec^{-2} isophote (S_{26}) vs. central surface brightness (S_0). Coding for the galaxies is the same as for Fig. 4. The solid lines represent the loci for exponential models with three different values of N.

In contrast, the mean surface brightness within a given isophote [in particular, S_{26} for the $S_{(T_1)} = 26$ mag arcsec^{-2} isophote] includes any feature departing from the model, but it may in turn be affected by the same drawbacks quoted for $T_{1_{26}}$.

If we deal only with "pure" exponential profiles (i.e., $N = 1$), S_{26} is a function of S_0 only, with no dependence on α, and consequently S_0 and S_{26} may be treated as equivalent (although S_0 varies faster than S_{26}). However, the introduction of a third parameter (N) causes S_{26} to vary with both S_0 and N; in this way, galaxies with similar values of S_0 but different N span a range in S_{26}, and the opposite (with similar values of S_{26}) is obviously also true, but with a broader range in S_0.

Figure 5 shows S_{26} as a function of S_0 for the dwarfs (*circles*) and for exponential models with three different values of N (*solid lines*). The striking feature in this graph is the narrow range that our dE's span in S_{26} compared with the relatively much broader range in S_0 (less than 1 mag arcsec^{-2} and 3 mag arcsec^{-2}, respectively; see Tables 2 and 3). A similar behavior can be noticed in other samples: CB87 give structural properties of 27 Fornax dE's spanning a range of 3.80 B mag arcsec^{-2} in central surface brightness (mean = 23.15, $\sigma = 0.77$), but only 2.10 mag arcsec^{-2} in $S_{27_{(B)}}$ (mean = 25.28, $\sigma = 0.42$), while the fainter sample of BIM comprises galaxies spanning a range of 1.49 mag arcsec^{-2} in $S_{0_{(B)}}$ (mean = 24.41; $\sigma = 0.43$) and 1.01 mag arcsec^{-2} in $S_{27_{(B)}}$ (mean = 25.95; $\sigma = 0.21$). Summarizing: Although the ranges in S_0 are wide and partially overlapping for the different samples, their S_{27} span narrower

ranges with a noticeable separation between their average values. The "extreme" LSB dwarfs of BIM conform, then, to a "family" with fainter average $S_{27_{(B)}}$ than the more "normal" dE's in CB87 or this work (recall that $T_1 = 26$ is nearly equivalent to $B = 27$ for these objects).

We conclude that the appearance of a given galaxy on a photographic plate (and therefore its inclusion in a sample to be observed with a CCD) seems then to be primarily determined not by its central surface brightness but by its average surface brightness. This point is relevant, since it may lead to selection effects, which we explore in the following subsection.

4.3. *Correlations and Selection Effects*

Our dE's fulfill the well-known relations between central surface brightness, total magnitude, and isophotal radius (Figs. 6 and 7); whether or not they are entirely produced by selection effects has already been widely discussed (Binggeli et al. 1984; CB87; DPCDK; Ferguson & Sandage 1988; IBM; Irwin et al. 1990), and little can be added to this discussion.

We have drawn in Figure 7 three curves (each corresponding to a different N) that trace the upper envelope in the relation r_{26} versus $T_{1_{tot}}$; no galaxy with a profile represented by equation (1) can exist above these curves. On the other hand, galaxies at the lower right in this figure (bright total magnitude and small isophotal radius) would be either compact and have high surface brightness or be extended and have very low surface brightness. Neither of these objects would have been included in our sample.

The relation between central surface brightness and total magnitude is mainly affected at faint magnitudes by the limiting diameter of the sample. Ferguson (1989) estimates that his catalog is complete down to a diameter of 17″ at $S_{(B)} \simeq 27$ mag arcsec^{-2} [or $S_{(T_1)} \simeq 26$ mag arcsec^{-2}], but we did not include in our sample very faint (and small) galaxies, so our limiting diameter is surely larger (or, alternatively, brighter). This effect is illustrated in Figure 6, where we have drawn a set of curves (labeled for three different values of N) corresponding to a limiting diameter of 34″ at $S_{(T_1)} = 26$ mag arcsec^{-2}, which act as boundaries to our data.

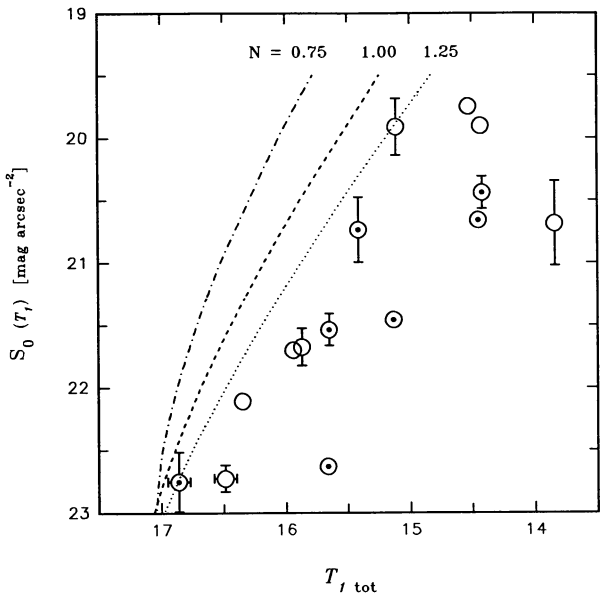

FIG. 6.—Central surface brightness (S_0) vs. total magnitude ($T_{1_{tot}}$); coding for galaxies is the same as for previous figures. Dash-dot, dashed, and dotted lines are tracks for exponential models with $N = 0.75$, $N = 1.00$, and $N = 1.25$, respectively, with isophotal diameters of 34″ at the $S_{(T_1)} = 26$ mag arcsec^{-2} level.

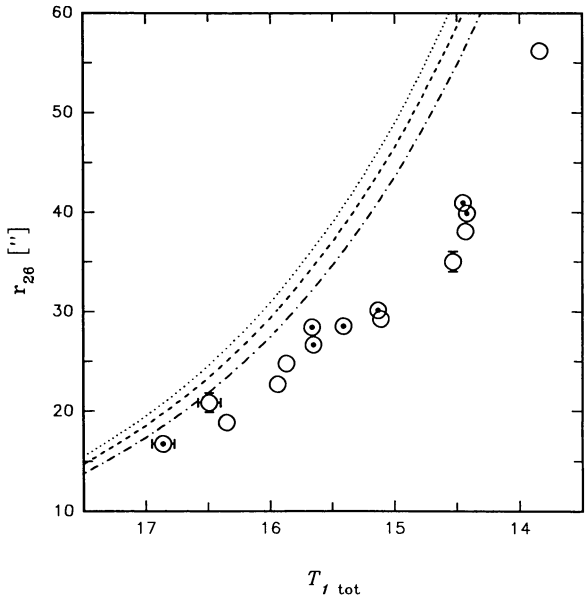

FIG. 7.—Radius of the $S_{(T_1)} = 26$ mag arcsec^{-2} isophote (r_{26}) vs. total magnitude ($T_{1_{tot}}$). The lines show the loci of exponential models with maximum r_{26} for a given total magnitude. The coding for the corresponding N-values is the same as for Fig. 6.

However, at bright magnitudes and faint central surface brightnesses, Figure 6 is free from selection effects, but it still shows a paucity of galaxies in that zone. Similar graphs in other works also show this feature (see, for example, Fig. 11 in BIM), and DPCDK allot it to the existence of a physical upper limit in the scale lengths α. Structural parameters for a possible galaxy "filling the gap" are given in the first line of Table 4 (we adopted $N = 1$, and we derived the corresponding α), and an artificial image (model 1, Fig. 9*a*) was created with these parameters. If a galaxy like model 1 existed in the Fornax Cluster, it would surely have been observed (note that its S_{26} is well within our boundaries and that r_{26} is quite large), so it may be that there are really no dE's in that region, although objects of a different type could exist. We have observed another Fornax member: NGC 1437A, a LSB late-type spiral, and our preliminary surface photometry shows that, although it has not a well-defined disk, its smooth light component is roughly exponential, with a central surface brightness $S_{0_{(T_1)}} = 21.4$ mag arcsec^{-2} and $T_{1_{tot}} = 13.5$ mag. These values place NGC 1437A very near model 1 in Figure 6, showing that there certainly are galaxies populating this region of the S_0-$T_{1_{tot}}$ plane, although their morphology is different from dE's.

Regarding the shape of the profiles, we mentioned in § 3 that there is qualitative evidence of fainter dwarfs having large cores while the brighter ones tend to have bulge components. Figure 8*a* shows this relation quantitatively: galaxies with $N <$

TABLE 4

MODEL PARAMETERS

Name	$S_{0(T_t)}$ (mag arcsec^{-2})	α	N	r_{26}	$T_{1_{tot}}$ (mag)	$S_{26(T_t)}$ (mag arcsec^{-2})
Model 1	22.00	15.″9	1.00	58.″51	14.00	24.21
Model 2	19.90	6.0	1.35	21.55	14.47	22.39
Model 3	22.75	9.0	0.75	38.83	15.23	24.88

1 (i.e., profiles more resembling a $r^{1/4}$ one) are the brighter ones, while the fainter dE's tend to have $N > 1$, which implies a curvature in the opposite sense.

We must now ask ourselves whether there are any selection effects artificially producing this relation. Our claim that galaxies are selected according to their similar mean surface brightnesses within a given isophote is not in conflict with IBM arguments, which are in turn based on Disney's (1976) assertion that, at a given total magnitude, galaxies with the largest isophotal size tend to be selected in photographic surveys. Following Allen & Shu (1979), the extrapolated central surface brightness of a galaxy whose r_{26} is maximum for its total luminosity is given by

$$S_0 = 26 - \frac{2.17}{N} . \quad (4)$$

As we have already mentioned, S_{26} depends only on S_0 and N; so, for galaxies with maximum isophotal radius, S_{26} will depend only on N. However, it can be shown that the dependence on N is weak, and so, at a given isophote, galaxies with the largest isophotal size for their luminosities will have similar average surface brightness.

Whatever point of view one adopts, there *seem to be* selection effects involved with the relation shown in Figure 8*a*. Keeping in mind the correlation between central surface brightness and total magnitude, one would expect N to correlate also with S_0; what is surprising in Figure 8*b* is that N is more tightly correlated with S_0 than with $T_{1_{tot}}$. However, in Figure 8*b*, galaxies with the same S_{26} lie on a single curve; so we have drawn the curves corresponding to $S_{26} = 23.5$ and $S_{26} = 24.6$, the lower and upper limits for our sample, respectively (*dashed lines*): one immediately sees that the selection of galaxies within the region bounded by these two curves automatically produces the correlation. The same information is already displayed in Figure 5; if the observed galaxies had values of N symmetrically distributed around a mean value (say $N = 1$), then they would follow the solid curves. Instead, there is a lack of higher surface brightness dwarfs with large N-values as well as of lower surface brightness dwarfs with small N-values.

Returning to Figure 8*b*, the dotted line shows the position of galaxies whose diameters are largest at a given isophote

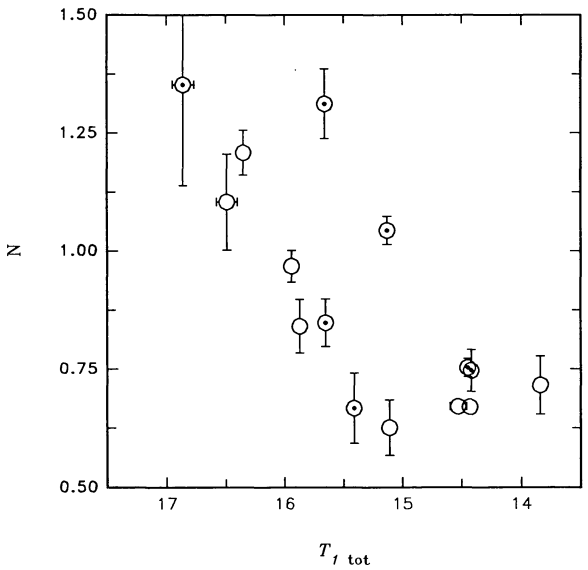

FIG. 8*a*

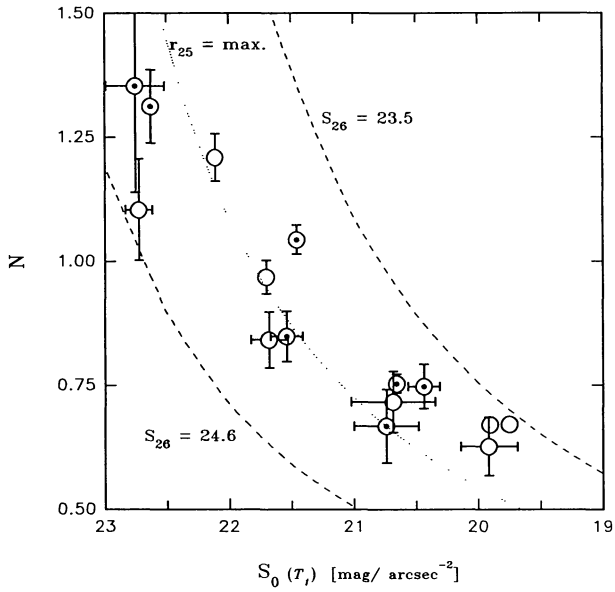

FIG. 8*b*

FIG. 8.—Shape parameter N (*a*) vs. total magnitude and (*b*) vs. central surface brightness. The dashed curves in (*b*) show the loci for exponential models with constant S_{26}, namely, at the 23.5 and 24.6 mag arcsec^{-2} levels. The dotted curve corresponds to exponential models with maximum isophotal diameter at the 25 mag arcsec^{-2} level.

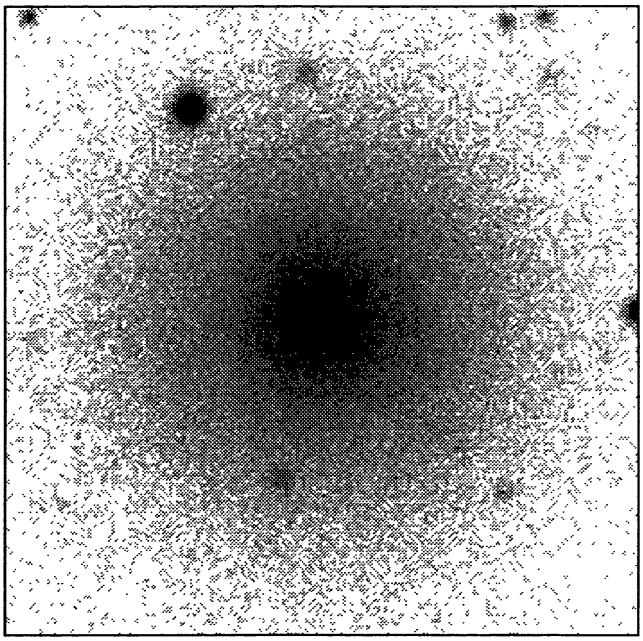

FIG. 9*a*

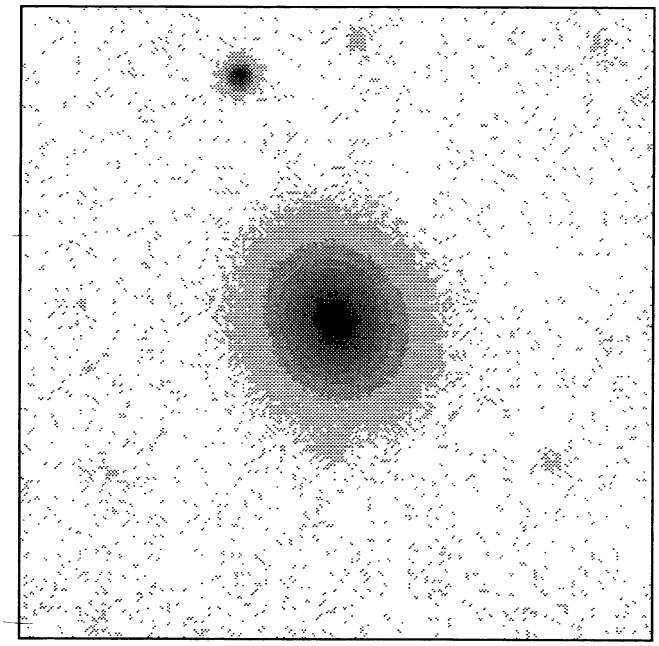

FIG. 9*b*

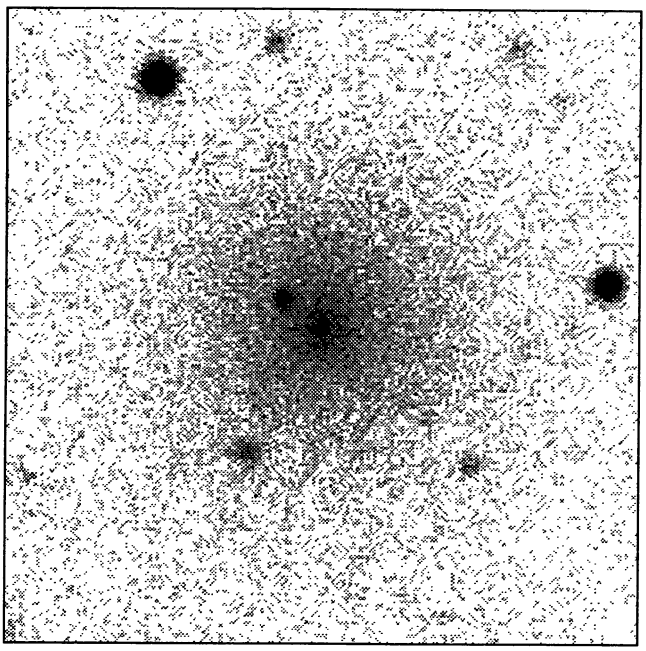

FIG. 9*c*

FIG. 9.—Gray-scale pictures of artificial galaxies added to an actual sky frame. Scale is the same as for Fig. 1. (*a*) Model 1; (*b*) model 2; (*c*) model 3.

(namely, the 25 mag arcsec^{-2} isophote; this isophote is brighter than the limiting one in F89 because we rejected very faint dwarfs). Our data seem to follow this curve, showing again that it is equivalent to speak about galaxies with maximum isophotal radius and galaxies with similar average surface brightness.

If one accepts that we were constrained by selection effects to observe galaxies within the mentioned boundaries, an interesting question should be asked: What would galaxies which lie *outside* of these boundaries look like? The last two lines in Table 4 list possible structural parameters for galaxies fulfilling that condition. In each case, the scale length α was appropriately selected to result in a "galaxy" large enough ($r_{26} > 17''$) to be included in the catalog (F89) and not too bright to be classified as a dwarf. Figures 9*b* and 9*c* show the images of two artificial galaxies created with these parameters and added to a true sky frame. A hypothetical galaxy such as model 2 in the Fornax Cluster would surely not have been classified as LSB; instead it would be indistinguishable from a bright background elliptical galaxy on a photographic plate. However, a large population of galaxies of this type must probably be ruled out, since background objects show no evidence of clustering in Ferguson's (1989) catalog and, on the other hand, there is no evidence of bright galaxies with N as high as 1.35 (but see the object labeled FLSBG 86 in Davies, Phillipps, & Disney 1990). Model 3 represents a more difficult problem: although we would probably have avoided galaxies like this one because of their low average surface brightness, there seems to be no a priori reason against their inclusion in fainter samples like that of BIM.

4.4. *The Nuclei*

Our sample is too small to derive any statistically significant conclusions about the nuclei, but a few interesting points can be made. Comparison of Figures 1 and 3 shows that, although a galaxy may appear to have a bright, resolved nucleus on a CCD image or a photographic plate, this is not always confirmed when one inspects its profile (see, for example, the frames of FCC 135 and FCC 195 and their corresponding profiles).

A nucleus, being a distinct structural component of a dE, must then be defined as a surface brightness enhancement above the extrapolation to the center of the galaxy's profile. This is a usual procedure, similar to the fitting of a bulge and a

disk component to the profile of a spiral galaxy. It is clear, then, that the only way to identify a nucleus definitively is from an accurate brightness profile. Still, a few dubious cases exist in our sample, and we have labeled them as "(Nuc)" in Table 2.

Identification of nuclei from photographic plates may be a very difficult and unreliable task. We have 14 dwarfs in common with Caldwell (1987), and we agree with his classification (i.e., nucleated or nonnucleated) in all but one galaxy and a dubious case (86%); but the degree of coincidence with other investigators is substantially lower: 67% with F89 and 64% with DPCDK. (Interestingly, the percentage of galaxies with similar classification in the last two studies is only 45%, even excluding those galaxies classified as background in F89.)

It has been claimed (Sandage, Binggeli, & Tammann 1985; van den Bergh 1986; IBM) that most of the brighter dE's are nucleated, and the fraction of nucleated dwarfs decreases with decreasing luminosity. However, as we have shown, the steep profile of a bright dE may be mistaken for a nucleus, and, on the other hand, fainter dwarfs, with "flatter" profiles ($N > 1$; see § 4.3), are easier to identify as nonnucleated. So it is not impossible that part of that correlation is an artifact of the difficulty in identifying nuclei on photographic plates. The same could be true for other investigations that discuss the properties of nucleated dwarfs, including their spatial distribution (Binggeli, Tammann, & Sandage 1987; IBM; Ichikawa et al. 1988; Ichikawa 1989; Ferguson & Sandage 1989); accurate CCD profiles should be the best way to resolve this question.

5. COLORS

5.1. *Color Profiles*

The standard $(C - T_1)$ and $(M - T_1)$ color profiles were obtained from the instrumental profiles for each band and the transformation equations discussed in § 3.2. Both colors are plotted against radius for each galaxy in Figure 3.

Looking for color gradients, one should take care in excluding the central regions (where seeing effects and the few pixels involved may give unreliable colors) as well as the outer regions, where the brightness profiles are poorly defined (as discussed in § 3.2). (A thoughtful discussion of errors involved in determining color gradients of LSB galaxies can be found in Vigroux et al. 1988.) Furthermore, care should be taken with two galaxies in particular: FCC 82, affected by relatively large residuals in the flat-field corrections, and FCC 296, which has a nearby star and was observed on a nonphotometric night, leading in both cases to spurious color gradients. Discarding these two galaxies, hardly any color gradient that cannot be due to small errors in the adopted sky level can be detected. The only exception is FCC 76, whose central region (out to $r \simeq 10''$) is remarkably bluer than its halo. The gradient is larger in $(C - T_1)$ than in $(M - T_1)$. However, this galaxy is morphologically quite different from the rest of our dwarfs; it is both the brightest and the biggest (see Table 3), and some blobs are evident near its center (see Fig. 1), possibly indicating some kind of recent star-forming activity. This conclusion is supported by the presence of emission lines in its spectrum (Jones & Jones 1980).

The absence of well-defined color gradients appears to be in conflict with Vader et al. (1988) and Davies et al. (1990) (see also the review by Peletier 1993), though in agreement with CB87. However, we have shown that the inclusion of galaxies with a different morphology (such as FCC 76) and the errors that inevitably arise when one studies these LSB objects may lead to ambiguous results.

The same reasons that were mentioned in the beginning of this section make it difficult to look for color differences between the nuclei and their surroundings. To do so, we performed aperture photometry on our images within a circular diaphragm 4″ in radius, and an annulus with inner and outer radii set to 4″ and 8″ respectively, both centered on the galaxies. The small diaphragm provides information on the central zone and is sufficiently large to avoid seeing errors (the seeing FWHM was typically 1.″4–1.″6), while the annulus is used to measure the colors of the surroundings.

In addition, integrated colors were derived as those which gave the best fit over most of the profile, excluding those regions mentioned above; the whole set of colors is listed in Table 5. As was expected, FCC 76 stands out with a notable color gradient: the galaxy is bluer within the small aperture and gets redder outward, both in $(C - T_1)$ and $(M - T_1)$.

For the rest of the dwarfs, colors measured within the annulus do not differ significantly from those measured from the whole profile, and only the faint ($T_{1_{tot}} > 15$) nonnucleated dE's are redder in $(C - T_1)$ at their centers. This effect does not show up in $(M - T_1)$, except for FCC 296 (contaminated by a star, as mentioned) and FCC 195, whose M frame was obtained with a bad focus. It is interesting to mention that Ostrov et al. (1993) find a metallicity gradient in the globular cluster system around NGC 1399. Their $(C - T_1)$ colors get bluer with increasing distance to the center of the galaxy, while the change in $(M - T_1)$ is not so large.

If we are not facing an odd combination of errors (mainly perhaps in flat-fielding and sky-level determination), then a possible scenario could be that faint dE's without nuclei have metallicities increasing toward their centers, while the brighter ones, along with nucleated dE's, either are more homogeneous or have age effects that cancel the metallicity effects. Alternatively, the average color difference in $(C - T_1)$ between the diaphragm and the annulus for these five galaxies (0.07 ± 0.03) is consistent with small amounts of dust producing color excesses $E_{B-V} = 0.03$. In any case, it is clear that the determination of color gradients in these small and low surface brightness objects is not straightforward and can be notably affected by instrumental errors.

5.2. *Correlations with Global Parameters*

Since color gradients are not prominent among these dwarfs, integrated colors, as defined in the last subsection, should reflect the properties of their dominant population.

Here we compare integrated colors with other global parameters. Figure 10 shows $(M - T_1)$ and $(C - T_1)$ plotted against $T_{1_{tot}}$: except for two galaxies (FCC 82 and FCC 296, whose color profiles are dubious as stated previously), $(M - T_1)$ is almost constant, spanning a narrow range, while $(C - T_1)$ tends to be redder for brighter galaxies (except for FCC 76, whose star-forming activity was already mentioned and will then not be included in the following discussion). A similar color-magnitude relation is found by CB87, although their $(U - V)$ colors have a large dispersion. Since $(C - T_1)$ is more sensitive to metallicity differences than $(M - T_1)$ (Geisler &

TABLE 5
COLORS

GALAXY (FCC)	DIAPHRAGM $r = 4''$		ANNULUS $4'' < r < 8''$		WHOLE PROFILE	
	$(M - T_1)$	$(C - T_1)$	$(M - T_1)$	$(C - T_1)$	$(M - T_1)$	$(C - T_1)$
76	0.56	1.15	0.58	1.23	0.61	1.37
82	0.84:	1.56	0.88:	1.54	0.83:	1.54
118	0.74	1.43	0.77	1.45	0.73	1.44
135	0.75	1.47	0.75	1.45	0.74	1.46
156	0.69	1.41	0.64	1.32	0.67	1.33
188	...	1.57	...	1.58	...	1.56
195	0.77:	1.56	0.69	1.52	0.68	1.50
201	0.71	1.42	0.75	1.39	0.72	1.34
203	0.74	1.57	0.73	1.59	0.70	1.57
222	0.75	1.60	0.74	1.62	0.73	1.61
250	0.71	1.54	0.66	1.43	0.68	1.44
274	0.67	1.39	0.64	1.43	0.64	1.42
296	0.92:	1.64	0.88:	1.57	0.86:	1.59
303	0.69	1.49	0.68	1.49	0.67	1.47
314	0.70	1.46	0.73	1.53	0.68	1.49

NOTE.—Colons indicate values suspected to be in error (see text).

Forte 1990), our data support the existence of a metallicity–absolute magnitude relation among Fornax dE's. A least-squares fit of $(C - T_1)$ to $T_{1_{tot}}$ has a correlation coefficient of 0.63. Recalling that total magnitudes correlate with central surface brightnesses and isophotal radii (Figs. 6 and 7), we should expect $(C - T_1)$ to correlate also with S_0 and r_{26} (the fact that the mentioned relations are due to selection effects is not relevant here); this assumption is confirmed in Figures 11 and 12.

There is no evidence for varying extinction across the Fornax Cluster (Burstein & Heiles 1982), so we adopted a uniform $E_{B-V} = 0.03$, or $E_{C-T_1} = 0.06$, using the reddening ratios of Harris & Canterna (1979). This value was chosen for homogeneity with Ostrov et al. (1993), although a smaller value (and even $E_{B-V} = 0.00$) is probably more widely accepted. In any case, the following conclusions are not changed. Our galaxies are then bracketed between $(C - T_1)_0 = 1.27$ and $(C - T_1)_0 = 1.55$, and, applying the calibration given in Geisler & Forte (1990) to these values, we obtain metallicities ranging from [Fe/H] = −1.40 to [Fe/H] = −0.75. Alternatively, the average color $\langle (C - T_1)_0 \rangle = 1.43 \pm 0.09$ (s.d.) gives a mean value of [Fe/H] = −1.04 with a standard deviation $\sigma = 0.20$ (excluding FCC 76). These values place the galaxies in the present sample at the bright end of the metallicity-luminosity relation already known for Local Group dwarf spheroidals (see Da Costa 1992 for a recent review). We show this relation in Figure 13, where the data for Local Group galaxies were taken from Caldwell et al. (1992), and absolute visual magnitudes for the Fornax Cluster dwarfs were calculated assuming $(V - T_1) = 0.3$ and adopting a Fornax-to-Virgo distance ratio $D_F/D_V = 0.93$ (Bothun et al. 1989) and a distance to the Virgo Cluster $D_V = 20.3$ Mpc (van den Bergh 1989). The solid line is the least-squares fit to the Local Group dwarfs shown by Caldwell et al. (1992) in their Figure 10. Clearly, the small disper-

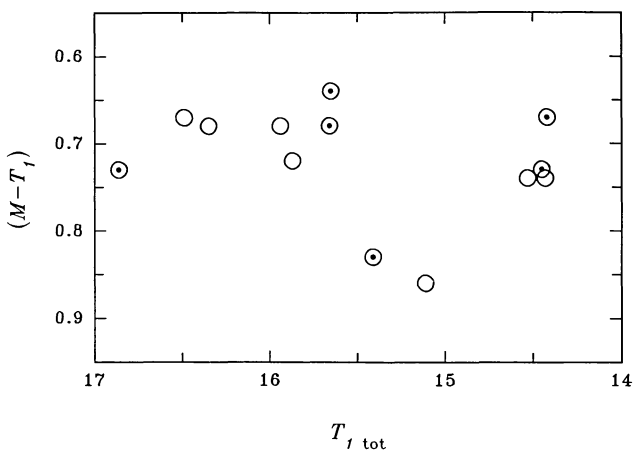

FIG. 10*a*

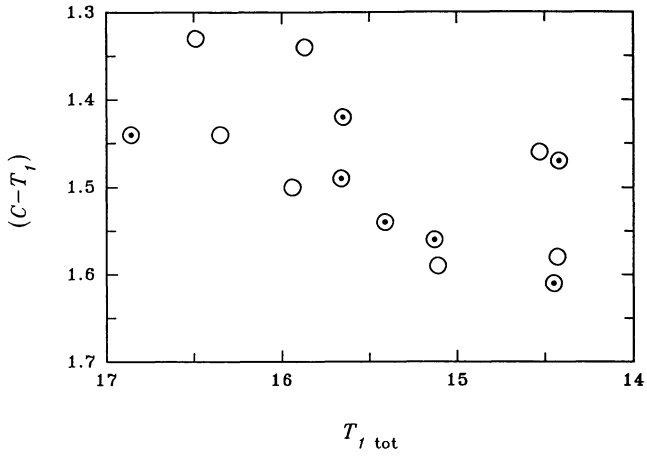

FIG. 10*b*

FIG. 10.—Integrated color vs. total magnitude (excluding FCC 76). (*a*) $(M - T_1)$; (*b*) $(C - T_1)$.

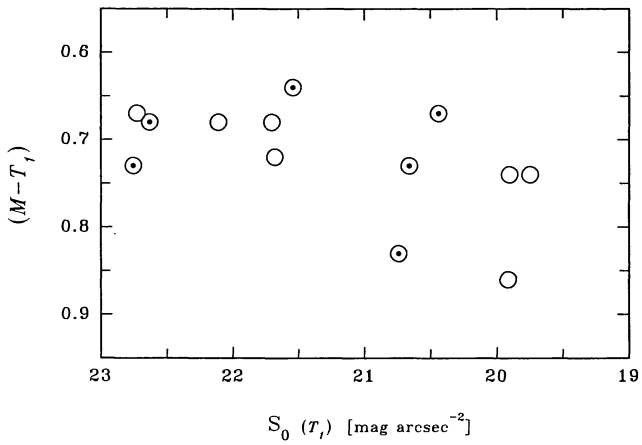

FIG. 11*a*

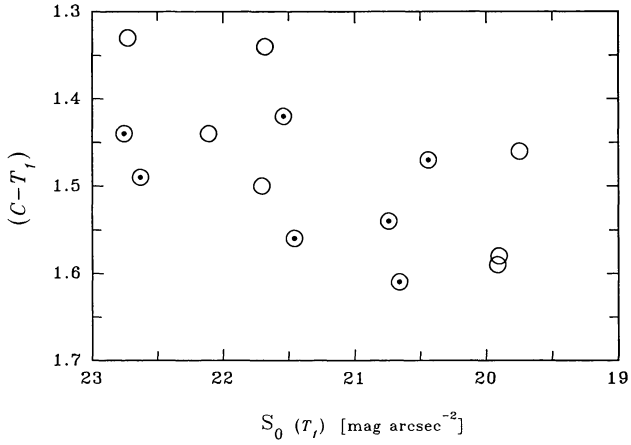

FIG. 11*b*

FIG. 11.—Integrated color vs. central surface brightness (excluding FCC 76). (*a*) $(M - T_1)$; (*b*) $(C - T_1)$.

sion about the mean [Fe/H] of our dwarfs is further reduced if we consider the dispersion with respect to this linear fit. This fact is in contrast to the results of Brodie & Huchra (1991), who measure abundances of Fornax and Virgo dwarf galaxies from their integrated spectra, finding a similar relation with absolute magnitude though with a much larger dispersion. Part of this larger dispersion may be due to the low signal-to-noise spectra of the dwarfs, but a substantial part is surely due to the inhomogeneity of their sample; only three out of a total of 10 galaxies that they observe in Fornax are classified as dE in F89. On the other side, we have two galaxies in common with their sample, and for both we derive higher abundances, though still within their quoted error margins.

It is interesting, then, to explore whether the rms scatter (amounting to 0.068 mag) in the $(C - T_1)$ versus $T_{1_{tot}}$ relation can be accounted for by observational errors alone. A conservative estimation of these gives individual values not larger than 0.035 mag, so it could be that there is a physical cause in the scatter. However, one should be cautious, since systematic errors could still be present. Bower, Lucey, & Ellis (1992) find a similar scatter in the relation between $U - V$ colors and total magnitudes for a sample of early (giant) galaxies in the Virgo and Coma clusters, but this scatter is reduced to a value small enough to be accounted for by observational errors when they restrict their sample to E galaxies, i.e., excluding S0 galaxies. So they conclude that there is no evidence for bright ellipticals having different star-forming histories. If we judge by our error estimates, this may not be the case with dE's. FCC 76 is in itself a good example of a galaxy too blue for its magnitude due to its recent star-forming activity.

On the other hand, the quoted mean $(C - T_1)_0$ of the dwarfs in this sample matches very closely the mean color ($\langle (C - T_1)_0 \rangle = 1.43$) of the outermost globular clusters around NGC 1399 given by Ostrov et al. (1993). These globulars exhibit a larger color dispersion than the dE's ($\sigma = 0.26$ and $\sigma = 0.09$, respectively), evidencing that they comprise objects with a larger spread in metallicities. Our data are then consistent with a dwarf's mean metal abundance being higher than that of the poorer globular clusters in NGC 1399, and close to the mean metal abundance of disk (i.e., metal-rich) Milky Way globu-

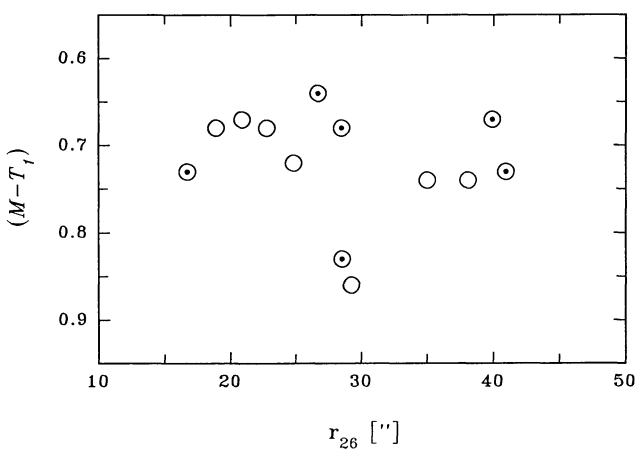

FIG. 12*a*

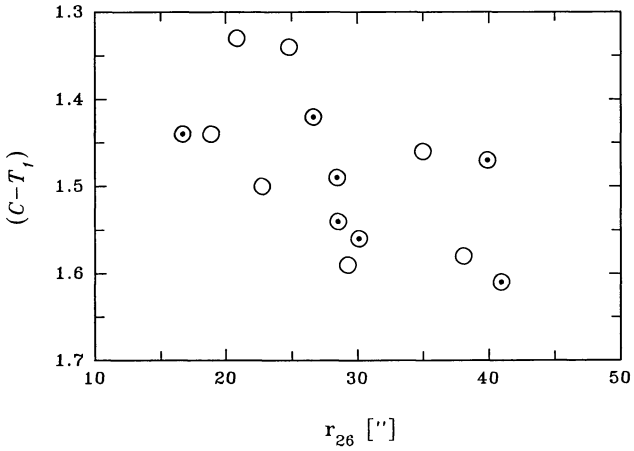

FIG. 12*b*

FIG. 12.—Integrated color vs. r_{26} (excluding FCC 76). (*a*) $(M - T_1)$; (*b*) $(C - T_1)$.

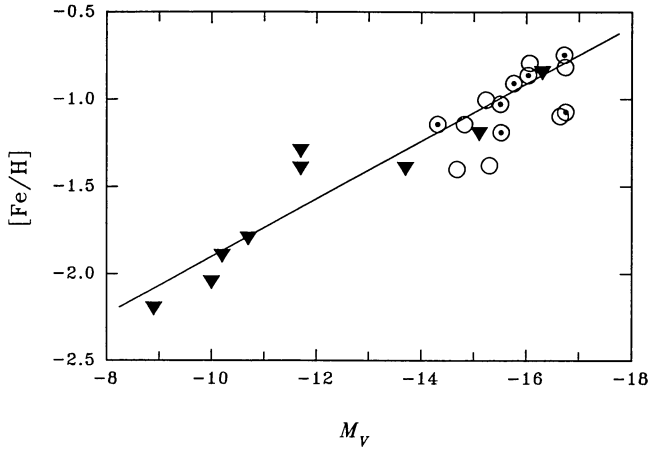

FIG. 13.—Metallicity vs. absolute visual magnitude. Circles are Fornax dE's from this work, while filled triangles are Local Group dwarfs from Caldwell et al. (1992). The solid line is a least-squares fit to the Local Group data (see text).

lars. However, we cannot discern whether the small spread in our derived metallicities is an intrinsic property of Fornax dE's, reflecting a more homogeneous origin compared with globulars, or is instead an effect due to the selection of galaxies with similar surface brightness. Accurate colors for a larger sample of dE's, including lower surface brightness ones, are surely needed to resolve these questions.

It is worth noting that no color segregation between nucleated and nonnucleated dwarfs is evident in Figure 10. This fact goes against the claim (CB87) that nucleated dE's with brighter nuclei tend to be redder. Again, a word of caution is needed regarding the identification of nuclei, given the large discrepancies found between different works (see § 4.4). Since various authors claim that the percentage of nucleated dE's decreases toward fainter magnitudes, and given that brighter dE's tend to be redder, the picture of nucleated dwarfs being redder immediately follows. So it may be that we are disentangling the effect of nuclei from that of luminosity, giving support to a color-magnitude relation as a fundamental one.

The general scenario is then that brighter dwarfs, which are in turn larger and with higher central surface brightnesses, tend to be more metal-rich. The question now is which parameter governs the star formation history of a dwarf galaxy. Several hypotheses were proposed. On the one hand, faint dwarfs are supposed to eject most of their gas during the supernova phase following their initial star formation burst, while more massive ones should have deep enough potential wells to retain part of their enriched gas, from which a second generation of higher metallicity stars could be formed (Larson 1974).

Alternatively, Phillipps, Edmunds, & Davies (1990) show a central surface brightness–metallicity relation extending from Virgo dE's to Local Group dSph's, and they connect this fact with the hypothesis that there is a threshold in the gas surface density (and, hence, the resulting stellar density) above which star formation can take place. However, as they point out, surface brightness decreases along the radius of a galaxy, and then, under certain assumptions, this relation should lead to metallicity gradients, in contrast to our observations. One would then have to look for a trend of metallicity with average surface brightness; in effect, our $(C - T_1)$ colors show a good correlation with S_{26}, but as S_{26} also correlates with S_0 (and therefore with $T_{1_{tot}}$), this adds little additional information. It is interesting to note that the relation of $(C - T_1)$ (and hence [Fe/H]) to S_0 (Fig. 11) has a higher dispersion than that with $T_{1_{tot}}$ (Fig. 10), in agreement with a similar (though marginal) effect found by Caldwell et al. (1992) for Local Group dSph's.

Finally, the stochastic self-propagating star formation models of Gerola, Seiden, & Schulman (1980) predict a color-size relation for dwarf galaxies, the smaller ones being redder, though with a larger dispersion in their colors. This prediction is just opposite to what we observe; however, we must recall that their models dealt with star-forming (i.e., gas-rich) dwarfs, and therefore blue *UBV* colors are representative of a recent star formation burst. In contrast, our dwarfs are of the elliptical type, which are shown to be gas-poor (Bothun et al. 1986), and then blue colors should reflect a low metal content (always excluding FCC 76). In this context, there is qualitative agreement between our Figure 12 and the metallicity-size relation predicted in Gerola et al. (1980).

5.3. *Colors and Projected Distances*

The projected distances of the dwarf galaxies in this sample to the Fornax Cluster center (adopted as the center of the distribution of the number density of member galaxies, given in F89) range from a few arcminutes to ~150′, i.e., from some 15 to ~840 kpc, with an assumed distance modulus $(m - M) = 31.4$, as quoted in § 5.2. It is interesting to explore whether there are any environmental effects acting upon the structure and colors of the dwarfs, though a larger sample would surely be necessary to derive firm conclusions.

Keeping in mind this drawback, our data show no trend of structural parameters with projected distance. However, something can be said about the colors: Figure 14 shows that, while no effect is observed in $(M - T_1)$, there is a lack of dwarfs with relatively red $(C - T_1)$ lying at large projected distances. This behavior is expected if the dwarfs have decreasing metallicity with increasing distance to the cluster's center; note that for small projected distances, a wide range of spatial distances is allowed. Although this fact may not represent any conclusive evidence, it is remarkable that, as was stated previously, a similar gradient exists among the globular clusters around NGC 1399.

6. CONCLUSIONS

Multicolor Washington surface photometry is presented for 15 dwarf elliptical galaxies in the Fornax Cluster. Radial surface brightness and color profiles as well as integrated colors were obtained, in order to investigate their structure and stellar populations.

Our observations show that the apparent flattenings do not vary with galactocentric distance, except for two of the brighter dwarfs whose inner isophotes are rounder. One of these two dwarfs also shows isophotal twisting, a feature that is not apparent in the rest of the sample. Such behavior indicates that morphological properties of dE's tend to join smoothly with those of bright ellipticals. A similar conclusion arises from the analysis of their surface brightness profiles, which generally depart from pure exponentials. The profile shape, quantified by a

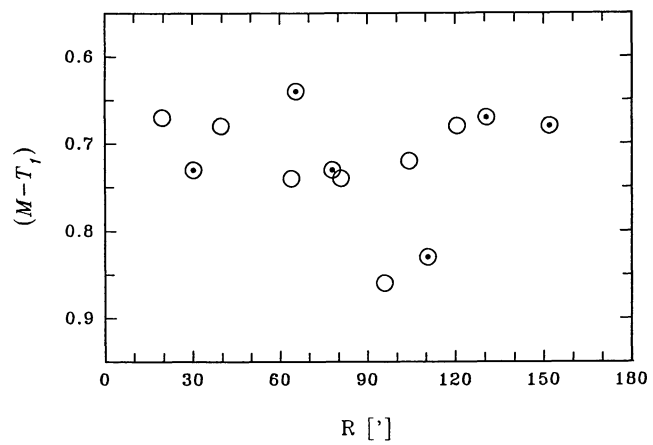

FIG. 14*a*

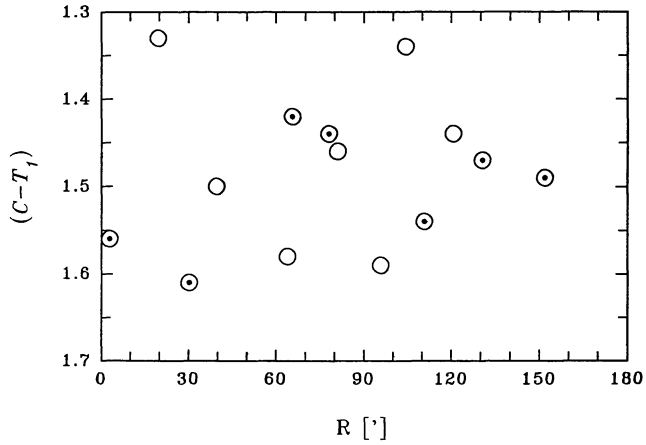

FIG. 14*b*

FIG. 14.—Integrated color vs. projected distance to the Fornax Cluster center, in arcminutes (excluding FCC 76). (*a*) $(M - T_1)$; (*b*) $(C - T_1)$.

third parameter (N) in the fitting formula, correlates with total magnitude: brighter dwarfs tend to have a bulge-type component, while fainter ones have "flat cores."

The well-known relation between central surface brightness and total magnitude is also found. Surely part of this correlation is due to selection effects; however, we show that there must be an actual paucity of relatively bright galaxies with low central surface brightnesses, but still having a dE-like morphology.

We then explore how galaxies are selected for a detailed study like the present one. We claim that the selection of dwarfs displaying a similar aspect on photographic plates, in order to conform to a homogeneous sample, implies the selection of galaxies spanning a very narrow range in average surface brightness within a certain isophote (the one at $T_1 = 26$ mag arcsec^{-2} in the present work). This effect leads to the observed correlation between the shape parameter N and central surface brightness, and hence with total magnitude. The existence of galaxies departing from this correlation is uncertain though rather unlikely, so the possibility that the correlation between total magnitude and N is real cannot be ruled out.

Regarding the bright nuclei observed in many dE's, we note that, on inspection of a photographic plate, or even a CCD image, the bright central region of a dwarf with a steep profile may be easily mistaken for a nucleus. On the other hand, any nucleus pops up immediately when the underlying galaxy has a shallow profile. These effects may bias any conclusion about nuclei derived without accurate CCD profiles.

For each dwarf, we derived color profiles and computed integrated colors. The Washington system index $(C - T_1)$ was used because of its particular sensitivity to metallicity. One of our galaxies (FCC 76) shows a blue central region, both in $(C - T_1)$ and in $(M - T_1)$, due to recent or current star-forming activity. The remaining dwarfs show no evident color gradient, or any significant color differences between central regions (including nuclei, when present) and outskirts. The fainter dE's without a nucleus are marginally redder in $(C - T_1)$ at their centers, suggesting a central metallicity enhancement.

Integrated colors show a distinct behavior when compared with global parameters: while $(M - T_1)$ is almost constant for the whole sample (excluding two galaxies likely to be in error), brighter galaxies (which are in turn larger and have higher central surface brightnesses) are redder in $(C - T_1)$. In this way, a metallicity-luminosity relation is derived for these Fornax dE's, in very close agreement with the similar relation known for Local Group early-type dwarfs. However, it is not clear which is the principal attribute (total magnitude, surface brightness, or size) that determines the final metallicity of a dE. Contrary to what is stated in other works, we find that nonnucleated dwarfs have the same colors as nucleated dwarfs of the same luminosity.

There is no evident trend of structural properties of the dwarfs (magnitude, surface brightness, size) with projected distance to the cluster center. Instead, there is a marginal shortage of dE's with red $(C - T_1)$ at large projected distances, in agreement with the existence of a metallicity gradient throughout the cluster of galaxies.

The average $(C - T_1)$ of our dwarfs (excluding FCC 76, for the reasons already stated) matches very closely the mean color of the outermost globular clusters around NGC 1399, but is bluer than the halo of this giant E galaxy at any distance from its center. These data are consistent with Fornax dwarfs having a heavy-element content similar to that of metal-rich Galactic globulars, and also suggest an evolutionary connection with the globular clusters around NGC 1399, within a picture similar to the one proposed by Searle & Zinn (1978) for the outer halo of the Galaxy.

REFERENCES

Allen, R. J., & Shu, F. H. 1979, ApJ, 227, 67
Bender, R., & Möllenhoff, C. 1987, A&A, 177, 71
Binggeli, B., Sandage, A., & Tammann, G. A. 1985, AJ, 90, 1681
Binggeli, B., Sandage, A., & Tarenghi, M. 1984, AJ, 89, 64
Binggeli, B., Tammann G. A., & Sandage, A. 1987, AJ, 94, 251
Binggeli, B., Tarenghi, M., & Sandage, A. 1990, A&A, 228, 42
Bothun, G. D., & Caldwell, N. 1984, ApJ, 280, 528
Bothun, G. D., Caldwell, N., & Schombert, J. M. 1989, AJ, 98, 1542

Bothun, G. D., Impey, C. D., & Malin, D. F. 1991, ApJ, 376, 404 (BIM)
Bothun, G. D., & Mould, J. R. 1988, ApJ, 324, 123
Bothun, G. D., Mould, J. R., Caldwell, N., & MacGillivray, H. T. 1986, AJ, 92, 1007
Bower, R. G., Lucey, J. R., & Ellis, R. S. 1992, MNRAS, 254, 589
Brodie, J. P., & Huchra, J. P. 1991, ApJ, 379, 157
Burstein, D., & Heiles, C. 1982, AJ, 87, 1165
Caldwell, N. 1983, AJ, 88, 804
———. 1987, AJ, 94, 1116
Caldwell, N., Armandroff, T. E., Seitzer, P., & Da Costa, G. S. 1992, AJ, 103, 840
Caldwell, N., & Bothun, G. D. 1987, AJ, 94, 1126 (CB87)
Canterna, R. 1976, AJ, 81, 228
Da Costa, G. S. 1992, in IAU Symp. 149, The Stellar Populations of Galaxies, ed. B. Barbuy & A. Renzini (Dordrecht: Kluwer), 191
Davies, J. I., Phillipps, S., Cawson, M. G. M., Disney, M. J., & Kibblewhite, E. J. 1988, MNRAS, 232, 239 (DPCDK)
Davies, J. I., Phillipps, S., & Disney, M. J. 1990, MNRAS, 244, 385
Disney, M. J. 1976, Nature, 263, 573
Ferguson, H. C. 1989, AJ, 98, 367 (F89)
Ferguson, H. C., & Sandage, A. 1988, AJ, 96, 1520
———. 1989, ApJ, 346, L53
———. 1990, AJ, 100, 1
Geisler, D. 1990, PASP, 102, 344
Geisler, D., & Forte, J. C. 1990, ApJ, 350, L5
Gerola, H., Seiden, P. E., & Schulman, L. S. 1980, ApJ, 242, 517
Harris, H. C., & Canterna, R. 1977, AJ, 82, 798
———. 1979, AJ, 84, 1750
Ichikawa, S.-I. 1989, AJ, 97, 1600
Ichikawa, S.-I., Okamura, S., Kodaira, K., & Wakamatsu, K.-I. 1988, AJ, 96, 62
Ichikawa, S.-I., Wakamatsu, K.-I., & Okamura, S. 1986, ApJS, 60, 475
Impey, C. D., Bothun, G. D., & Malin, D. F. 1988, ApJ, 330, 634 (IBM)
Irwin, M. J., Davies, J. I., Disney, M. J., & Phillipps, S. 1990, MNRAS, 245, 289
Jones, J. E., & Jones, B. J. T. 1980, MNRAS, 191, 685
Karachentseva, V. E., Karachentsev, I. D., & Börngen, F. 1985, A&AS, 60, 213
Karachentseva, V. E., Karachentsev, I. D., Richter, G. M., von Berlepsch, R., & Fritze, K. 1987, Astron. Nach., 308, 247
Karachentseva, V. E., Schmidt, R., & Richter, G. M. 1984, Astron. Nach., 305, 59
Larson, R. B. 1974, MNRAS, 169, 229
Ostrov, P., Geisler, D., & Forte, J. C. 1993, AJ, 105, 1762
Peletier, R. F. 1993, ESO Sci. Preprint 872
Phillipps, S., Edmunds, M. G., & Davies, J. I. 1990, MNRAS, 244, 168
Reaves, G. 1983, ApJS, 53, 375
Sandage, A., Binggeli, B., & Tammann, G. A. 1985, AJ, 90, 1759
Searle, L., & Zinn, R. 1978, ApJ, 225, 357
Thuan, T. X. 1985, ApJ, 299, 881
Vader, J. P., Vigroux, L., Lachièze-Rey, M., & Souviron, J. 1988, A&A, 203, 217
van den Bergh, S. 1986, AJ, 91, 271
———. 1989, Astron. Astrophys. Rev., 1, 111
Vigroux, L., Souviron, J., Lachièze-Rey, M., & Vader, J. P. 1988, A&AS, 73, 1